國 立 交 通 大 學

工學院聲音與音樂創意科技碩士學位學程

碩士論文

耳機聲學最佳化設計與全向性聲源設計

Optimized Design of Earphone Enclosures and Omni-Directional Source Design

研 究 生：廖士涵

指導教授：白明憲

中華民國九十九年七月

耳機聲學最佳化設計與全向性聲源設計

Optimized Design of Earphone Enclosures and Omni-Directional Source Design

研 究 生：廖士涵　　Student：Shih Han Liao

指導教授：白明憲　　Advisor：Ming sian Bai

國 立 交 通 大 學

工 學 院 聲 音 與 音 樂 創 意 科 技 碩 士 學 位 學 程

碩 士 論 文

A Thesis

Submitted to Master Program of Sound and Music Innovative Technologies

College of Engineering

National Chiao Tung University

in partial Fulfillment of the Requirements

for the Degree of

Master

in

Engineering

July 2010

Hsinchu, Taiwan, Republic of China

中華民國九十九年七月

耳機聲學最佳化設計與全向性聲源設計

研究生：廖士涵　　指導教授：白明憲 教授

國立交通大學

工學院聲音與音樂創意科技碩士學位學程

摘　　要

面對耳機設計時各種相互衝突的特性需求，如靈敏度、失真率、頻寬以及微小化等，需要一種有系統且有效率的方法來達成我們的設計並符合設計需求。利用微型揚聲器的參數鑒別法、電機聲模擬電路 (EMA)，建立耳機的聲學模擬平台。並且以此平台為基礎，利用模擬退火法 (simulated annealing)進行耳機腔體的最佳化設計，並能有效達到期望目標。實驗方面，利用 Type 3.3 人工耳（IEC 711 ear simulator）來得到實驗結果，並且顯示出經最佳化後的耳機腔體設計，能夠大大的提升其聲學品質，並且能夠符合 3GPP2 的規範。

全向性聲源在某些特定的聲學測量和音訊重現應用中是有需要的，在本篇論文中，把十二個動圈式喇叭分別鑲嵌到鋁製正十二面體的十二個面上，形成一個十二面體揚聲器來近似全向性聲源。為了預測指向性，利用等效聲源法(ESM)來建構此十二面體揚聲器的模型，利用此模型來模擬遠場聲壓，實際上的量測，是採用旋轉桌(turn table)量測水平面 360^0 的聲壓分佈，由實驗跟模擬上的結果，可以顯現出此正十二面體揚聲器的性能，非常接近全向性聲源。

Optimized Design of Earphone Enclosures and Omni-Directional Source Design

Student: Shih Han Liao Advisor: Mingsian R. Bai

Master Program of Sound and Music Innovative Technologies

National Chiao-Tung University

ABSTRACT

Faced with various conflicting issues arising from sensitivity, distortion, bandwidth and miniaturization requirements for earphones, it is desirable to develop a systematic way to attain the design that would meet these requirements. Based on a lumped parameter model, the design of the earphone enclosure is optimized using the simulated annealing (SA) algorithm. Experimental results obtained using a type 3.3 artificial ear (IEC 711 ear simulator) reveals that the optimized design has resulted in significant enhancement of performance, complying with the frequency response mask dictated in the 3GPP2 standard.

Omni-directional sources are required in some special acoustical measurements as well as audio reproduction applications. This thesis aims to design a dodecahedral loudspeaker source to approximate an omni-directional source. Twelve drivers are mounted in an enclosure made of stainless steel. In order to predict the directional response, the equivalent source method (ESM) is employed to calculate the pressure radiation pattern of the source. In addition to the numerical simulation, practical measurement of the directional response was performed using the turn table. Both numerical and experimental results show demonstrated the satisfactory omni-directional property of the source.

誌謝

時光飛逝，短短兩年的研究生生涯轉眼就過去了。首先感謝指導教授白明憲博士的諄諄指導與教誨，使我順利完成學業與論文，在此致上最誠摯的謝意。而老師指導學生時豐富的專業知識，嚴謹的治學態度以及待人處事方面，亦是身為學生的我學習與景仰的典範。

在論文寫作上，感謝本系鄭泗東教授和謝世福教授在百忙中撥冗閱讀並提出寶貴的意見，使得本文的內容更趨完善與充實，在此本人致上無限的感激。

回顧這兩年的日子，承蒙同實驗室的林家鴻學長、陳勁誠學長、郭育志學長、王俊仁學長、劉冠良學長、何克男學長以及艾學安學長在研究與學業上的適時指點，並有幸與廖國志、張濬閣、桂振益、曾智文、陳俊宏及劉嬰婷同學互相切磋討論，每在烏雲蔽空時，得以撥雲見日，獲益甚多。此外學弟吳俊慶、王俊凱、徐偉智、衛帝安及許書豪在生活上的朝夕相處與砥礪磨練，都是我得以完成研究的一大助因，在此由衷地感謝他們。

能有此刻，我也要感謝所有在精神上給我鼓舞支持的人，謝謝各位的幫忙與鼓勵。最後僅以此篇論文，獻給我摯愛的雙親廖榮裕先生、陳淑蘋女士、弟弟廖崇祐。今天我能順利取得碩士學位，要感謝的人很多，上述名單恐有疏漏，在此也一致上我最深的謝意。

Table of Contents

LIST of TABLES

LIST of FIGURES

1. Introduction

Firstly, in recent years, electro-acoustical transducers have become key components to many 4C (Computer, Communication, Consumer electronics and Car) products. Therefore, miniaturization is the trend of the 4C portable devices such as mobile phones, personal digital assistants (PDAs), MP3 player, earphone, etc. And sound quality is an important part. This essay introduces the design of earphone. Measure and simulate electro- acoustical transducer by using EMA analogous circuits. Secondly, conventional loudspeaker systems consist of drivers mounted in an enclosure and the sound pressure is limited in special range on one direction. It is a disadvantage of those loudspeaker systems used in some special surroundings. Therefore, the omni-directional source has been designed by using ESM model.

The characteristics of micro-speakers have been studied extensively in a variety of aspects, including the structure dynamics of the diaphragm, the voice-coil impedance properties of cover perforation [1]-[4], electronic compensation [5], and structural optimization [6]. A well-known method to model of dynamic moving-coil micro-speakers is through the use of the EMA analogy. Lumped parameter models can be established, with the aid of such approach [7]-[9].The Thiele and Small (T-S) parameters of the micro-speaker need to be experimentally identified prior to the response simulation [10]. Using the analogous circuit, the dynamic responses of micro-speaker can readily be simulated, enabling the ensuing design [11].

Earphones have become an important accessory for reproducing speech in hands-free communication and consumer electronics. Faced with various conflicting issues arising from sensitivity, distortion, bandwidth and miniaturization requirements, it is desirable to develop a systematic and efficient way to attain the design that would meet these requirements.

In this thesis, EMA analogous circuit is used to model a Bluetooth earphone.

Thiele and Small (T-S) parameters of the microspeaker embedded in the earphone are experimentally identified. Thus, for the microspeaker and the associated enclosure and casing, a lumped parameter model can be established to predict the frequency response. On the other hand, acoustical impedance of ear canal that is distinct from a free-field environment is also incorporated into the model.

As mentioned previously, it is vital to optimize the enclosure design for a given driver such that the requirements are met. To this end, the Simulated Annealing (SA) [12] is employed to search for the optimal combination of enclosure parameters. SA is a random-search technique which exploits an analogy between the way in which a metal cools and freezes into a minimum energy crystalline structure (the annealing process) and the search for a minimum in a more general system. Using the forgoing lumped parameter model, the sound pressure response at the ear drum position can be simulated for the SA optimization. The cost function alongside the constraints posed by practical application and implementation are formulated in accordance with the frequency response mask dictated in the standard of 3GPP2 C.S0056-0 [13]. A mockup is made based on the optimal design. Experimental results obtained using a type 3.3 ear simulator [14]-[15] are discussed in the conclusions.

Traditionally, most of loudspeaker systems consist of drivers mounted in an enclosure and the sound pressure is limited in special range on one direction which becomes increasingly directional with frequency. It is a disadvantage of those loudspeaker systems to use to be a source in some special surroundings such as reverberant field evaluation [16], head related transfer function (HRTF) measurement [17], digital band performance. A simple way to avoid this disadvantage is eliminating the directivity from speaker system. Therefore, the omni-directional speaker has been designed to meet the above requirements. A perfect omni-directional source should be like a point source which could product spherical

sound wave. The sound wave propagation of omni-directional speaker is considered to be a perfect sphere in three dimensions. Designing an ideally omni-directional source is very difficult to achieve not only the cost but also the mechanical limitation. Therefore, the other geometric structure should be adopted to design the omni-directional source. In this thesis, the structure of omni-directional source is designed as a regular dodecahedron comprising twelve regular pentagonal faces with three meeting at each vertex.

The Equivalent Source Method (ESM) [18]-[21] also known as wave superposition method [22]-[24], was suggested for sound field calculation with far less complexity and had higher computational efficiency than the other methods such as Boundary Element Method (BEM) [25]-[26] and Finite Element Method (FEM) [27]. The idea underlying the ESM is to represents sound field with discrete simple sources with no need to perform numerical integration. As opposed to the actual source, these simple sources are solutions of the acoustic wave equation and pose only in virtual sense for field representation purpose. In this thesis, the ESM is used to establish the regular dodecahedron model. The numerical and experimental results are discussed and summarized in the conclusions.

2 Theory and Method

A loudspeaker is an electroacoustic transducer that converts the electrical signal to sound signal. The processes of the transduction are complex. These cover the electrical, mechanical, and acoustical transduction. In order to model the process of the transduction, the EMA analogous circuit can be used to simulate the dynamic behavior of the loudspeaker. The circuit is overall and decomposed to electrical, mechanical, and acoustic part. A loudspeaker is characterized by a mixed of electrical, mechanical, and acoustical parameters.

2.1 Electrical-mechanical-acoustical analogous circuit

The concept of the electric circuit often applied to analyze transducers in the electrical and mechanical system. The technique analysis of the electric circuit can be adopted to analyze the transduction of the mechanical and acoustical system. The simple diagram of EMA analogous circuit is shown in Fig. 1. The subject of EMA analogous circuit is the application of electrical circuit theory to solve the coupling of the electrical, mechanical and acoustical system. The EMA analogous circuit is formulated by the differential equations of the electrical, mechanical, and acoustical system and the differential equations can be modeled by the circuit diagram. The rules of analytic methods are follows. For the electromagnetic loudspeaker, the diaphragm is driven by the voice coil. The voice coil has inductance and resistance which are defined R_E and L_E . The term R_E and L_E are the most common description of a loudspeaker's electrical impedance. In order to model the nonlinearity of inductance, a resistance R'_E can be parallel connected to inductance. Thus, the electrical impedance of loudspeaker is formulated as:

$$Z_E = R_E + (j\omega L_E \,//\, R'_E) \tag{1}$$

When the current (i) is passed through the voice coil, the force (f) is produced and that drives the diaphragm to radiate sound. The voltage (e) induced in the voice coil when it movies with the mechanical velocity (u) . The basic electromechanical equations that relate the transduction of the electrical and mechanical system are listed.

$$f = Bli \tag{2}$$

$$e = Blu \tag{3}$$

Here, electro-mechanical transduction can be modeled by a gyrator. So, the loudspeaker impedance is formulated as:

$$Z = \frac{e}{i} = Z_E + \frac{Bl^2}{Z_M + Z_{MA}} \tag{4}$$

where Z_M is the mechanical impedance and Z_{MA} is the acoustical impedance reflecting in mechanical system as shown in Fig. 1(b).

A simple driver model is shown in Fig. 2. This simple driver model can be used to describe the mechanical dynamics of the electromagnetic loudspeaker. Force f is produced according to the Eqs. (2). Vibration of the diaphragm of the loudspeaker displaces air volume at the interface. The primary parameters of the simple driver are the mass, compliance (compliance is the reciprocal of stiffness) and damping in the mechanical impedance. The acoustical impedance is induced by the radiation impedance, enclosure effect and perforation of the enclosure. f_S is the force that air exerts on the structure. The coupled mechanical and acoustical systems can be simplified as :

$$M_{MD}\ddot{x} = f - \frac{x}{C_{MS}} - R_{MS}\dot{x} - f_S \tag{5}$$

where M_{MD} is the mass of diaphragm and voice coil, f is the force in newtons, f_S is the force that air exert on the structure, C_{MS} is the mechanical compliance, R_{MS} is the mechanical resistance and x is the displacement.

$$M_{MD}(s)(j\omega)^2 x(s) = f(s) - \frac{x(s)}{C_{MS}} - R_{MS} j\omega x(s) - f_S \quad (6)$$

$$M_{MD}(s) j\omega u(s) = f(s) - \frac{u(s)}{j\omega C_{MS}} - R_{MS} u(s) - f_S$$

$$f = (Z_M + Z_A) u(s) \quad (7)$$

where $Z_M = j\omega M_{MD} + R_{MS} + \frac{1}{j\omega C_{MS}}$ is the mechanical impedance and Z_A is the acoustical impedance.

$$f_S = Z_A u \quad (8)$$

The acoustical impedance primarily includes radiation impedance, enclosure impedance, and perforation of the enclosure. The acoustical impedance can be formulated as:

$$Z_A = Z_{AF} + Z_{AB} \quad (9)$$

The general acoustic circuit is shown in Fig. 3(a). The Z_{AF} means the impedance in the front of diaphragm and Z_{AB} means that in the back side. In general, the circuit would turn to Fig. 3(b) the general form in the electronics. The following discussion will use this kind of circuit.

The two basic variables in acoustical analogous circuit are pressure p and volume velocity U. Because of using impedance analogy, the voltage becomes pressure p and current becomes volume velocity U. Therefore, the ground of this circuit showing in Fig. 3 means the pressure of the free air. Thus, it also can employ the concept about the mechanical system and the acoustical system can be coupled by the below two equations.

$$f_S = S_D p \quad (10)$$

$$U = S_D u \quad (11)$$

The equation $f_S = S_D p$ represents the acoustic force on the diaphragm generated by the difference in pressure between its front and back side, where S_D is the effective diaphragm area and p is the difference in acoustic pressure across the

diaphragm. The volume velocity source $U = S_D u$ represents the volume velocity emitted by the diaphragm. From the Eqs. (10), the pressure difference between the front and rear of the diaphragm is given by

$$p = U(Z_{AF} + Z_{AB}) \tag{12}$$

Using Eqs. (10) and (11), force field can be transformed to pressure field.

2.2 The method of parameter identification

Almost all of the useful loudspeaker parameters had been defined by other researchers before Thiele and Small. However, Thiele and Small made these parameters in a complete design approach and shown how they could be easily determined from impedance data. There are at least four methods for measuring Thiele and Small parameters from driver impedance data. They are:

1. Closed box (Delta compliance method)
2. Added mass (Delta mass method)
3. Open box only
4. Open box/closed box

The first two procedures are the most popular. But for miniature speaker, the closed box method is the best choice. The closed box method and curve fitting method are adopted to calculate the Thiele and Small parameters. Placing the driver in a closed box will induce the alteration of the resonant frequency. The curve fitting employs the impedance of system to calculate the parameters of Thiele and Small precisely. Both methods are explained in the following section.

Curve fitting method

The curve fitting method is used to calculate Q_{ES} and the result is more accurate. The procedure of the curve fitting method is explained as follows.

(a) Choose the $(\frac{1}{j\omega M + R + \frac{1}{j\omega C}})$ to be become the basic element that it fit a peak of the impedance curve. Because the purpose of the method is to fit the mechanical part, the electrical part can be obtained previously.

(b) Choose the fitting range in the impedance curve. If the range of the impedance curve is chosen broadly, result of the fitting is poor. Therefore, the range that starts and ends both sides of peak enclosures the peak, and it can be chosen. Then, the peak will fit better and it is obtained second order system transfer function.

(c) We compare the coefficient between the second order transfer function and $\frac{1}{s^2 + 2\xi\omega_s + \omega_s^2}$, then the parameters ω_s and Q_{MS} are solved.

$$\omega_s = 2\pi f_S$$

$$Q_{MS} = \frac{1}{2\xi} \tag{13}$$

$$Q_{ES} = Q_{MS}(\frac{R_E}{R_{ES}}) \tag{14}$$

Closed box method

When the impedance of a mechanical system is $Z_M = j\omega M_{MS} + R_{MS} + \frac{1}{j\omega C_{MS}}$ the resonant frequency is $\omega_s = \frac{1}{\sqrt{M_{MD} C_{MS}}}$. When a driver is placed in a closed box, its resonant frequency rises. This is because the inward cone motion is resisted not only by the compliance of its own suspension, but also by the compression of the air in box. The compliance of the driver suspension is reduced by the compliance of the air spring. If the total compliance has decreased, the resonant frequency of the driver will rise. The concept can employed to calculate to the mechanical mass, mechanical compliance and mechanical resistance of the system.

The closed box procedure for determining T/S parameters is given below:

1. Measure f_S and Q_{ES} using the curve fitting method
2. Mount the driver in the test box. Make sure there are no air leaks around the box and speaker. One point must be noticed is that the testing volume for the case of miniature speaker must be less than 0.015L, or you can't measure the realizable T/S parameters.
3. Measure the new in-box resonant frequency and electrical *Q* using the same procedure as that used in step 1. Label these new value f_C and Q_{EC} .
4. Compute the V_{AS} as follows:

$V_{AS} = V_T(\frac{f_C Q_{EC}}{f_S Q_{ES}} - 1)$ Where V_T is the total volume of the tested box

Therefore, the mechanical mass M_{MD} and mechanical compliance C_{MS} can be solved as

$$C_{MS} = \frac{V_{AS}}{\rho_0 c^2 S_D^2} \tag{15}$$

$$M_{MS} = \frac{V_{AS}}{\omega_S^2 C_{MS}} \tag{16}$$

$$M_{MD} = M_{MS} - 2M_1 \tag{17}$$

where M_1 is the air-load impedance at low frequency.

On the other hand, the parameters, and the mechanic resistance ($_{MS}R$) and the motor constant (*Bl*) can be calculated, using the following formula:

$$R_{MS} = \frac{\omega_S M_{MS}}{Q_{MS}} \tag{18}$$

$$Bl = \sqrt{\frac{\omega_S R_E M_{MS}}{Q_{MS}}} \tag{19}$$

And the lossy voice-coil inductance can be calculated, using the following method:

$$Z_E(j\omega) \approx (j\omega)^n L_E$$

$$R_E^{'} = \left[\frac{L_e}{\cos(n\pi/2)}\right]\omega^n, L_E = \left[\frac{L_e}{\cos(n\pi/2)}\right]\omega^{n-1} \tag{20}$$

(n=1:inductor;n=0:resistor)

The parameters n and L_e can be determined from one measurement of Z_{VC} at a frequency well above f_s, where the motional impedance can be neglected

$$Z_E = Z_{VC} - R_E$$

$$n = \frac{1}{90}\tan^{-1}\left[\frac{\mathrm{Im}(Z_E)}{\mathrm{Re}(Z_E)}\right] = \frac{\ln|Z_2| - \ln|Z_1|}{\ln\omega_2 - \ln\omega_1}\ ,\ L_E = \frac{|Z_E|}{\omega^n} \tag{21}$$

The method to calculate lossy voice-coil inductance is described [28].

2.3 Modeling Acoustical Systems

Electroacoustics is using the analogous circuit to model the acoustical behavior including acoustic mass, acoustic resistance and acoustic compliance. The impedance type of analogy is the preferred analogy for acoustical circuits. The sound pressure is analogous to voltage in electrical circuits. The volume velocity is analogous to current.

Acoustic Resistance

Acoustic resistance is associated with dissipative losses that occur when there is a viscous flow of air through a fine mesh screen or through a capillary tube. Fig. 4(a) illustrates a fine mesh screen with a volume velocity U flowing through it. The pressure difference across the screen is given by $p = p_1 - p_2$, where p_1 is the pressure on the side that U enters and p_2 is the pressure on the side that U exits. The pressure difference is related to the volume velocity through the screen by

$$p = p_1 - p_2 = R_A U \tag{22}$$

where R_A is the acoustic resistance of the screen. The circuit is shown in Fig. 4(b).

Theoretical formulas for acoustic resistance are generally not available. The values are usually determined by experiments. Table 1 gives the acoustic resistance of typical screens as a function of the area S of the screen, the number of wires in the screen, and the diameter of the wires.

Acoustic compliance

Acoustic compliance is a parameter that is associated with any volume of air that is compressed by an applied force without an acceleration of its center of gravity. To illustrated an acoustic compliance, consider an enclosed volume of air as illustrated in Fig. 5(a). A piston of area S is shown in one wall of the enclosure. When a force f is applied to the piston, it moves and compresses the air. Denote the piston displacement by x and its velocity by u. When the air is compressed, a restoring force is generated which can be written $f = k_M x$, where k_M is the spring constant. (This assumes that the displacement is not too large or the process cannot be modeled with linear equation.) The mechanical compliance is defined as the reciprocal of the spring constant. Thus we can write

$$f = k_M x = \frac{x}{C_M} = \frac{1}{C_M}\int u dt \tag{23}$$

This equation involves the mechanical variables f and u. We convert it to one that involves acoustic variables p and U by writing $f = pS$ and $u = U/S$ to obtain

$$p = \frac{1}{S^2 C_M}\int U dt = \frac{1}{C_A}\int U dt \tag{24}$$

This equation defines the acoustic compliance C_A of the air in the volume. It is

given by

$$C_A = S^2 C_M \tag{25}$$

An integration in the time domain corresponds to a division by $j\omega$ for phasor variable. It follows from Eqs. (24). That the phasor pressure is related to the phasor volume velocity by $p = \frac{U}{j\omega C_A}$. Thus the acoustic impedance of the compliance is

$$Z_A = \frac{p}{U} = \frac{1}{jwC_A} \tag{26}$$

The impedance which varies inversely with $j\omega$ is a capacitor. The analogous circuit is shown in Fig. 5(b). The figure shows one side of the capacitor connected to ground. This is because the pressure in a volume of air is measured with respect to zero pressure. One node of an acoustic compliance always connects to the ground node. The acoustic compliance of the volume of air is given by the expression derived for the plane wave tube. It is

$$C_A = \frac{V}{\rho c^2} \tag{27}$$

Acoustic mass

Any volume of air that is accelerated without being compressed acts as an acoustic mass. Consider the cylindrical tube of air illustrated in Fig. 6(a) having a length l and cross-section S. The mss of the air in the tube is M_0 $M_M = \rho_0 Sl$. If the air moved with velocity u, the force required is given by $f = M_M \, du/dt$. The volume velocity of the air through the tube is $U = Su$ and the pressure difference between the two ends is $p = p_1 - p_2 = f/S$. It follows from these relations that the pressure difference p can be related to the volume velocity U as follows:

$$p = p_1 - p_2 = \frac{M_M}{S}\frac{du}{dt} = \frac{M_M}{S^2}\frac{dU}{dt} = M_A \frac{dU}{dt} \tag{28}$$

where M_A is the acoustic mass of the air in the volume that is given by

$$M_A = \frac{M_M}{S^2} = \frac{\rho_0 l}{S} \tag{29}$$

A differentiation in the time domain corresponds to a multiplication by $j\omega$ for sinusoidal phasor variable. If follows from Eqs. (28) that the phasor pressure is related to the phasor volume velocity by $p = j\omega M_A U$. Thus the acoustic impedance of the mass is

$$Z_A = \frac{p}{U} = j\omega M_A \tag{30}$$

An electrical impedance which is proportional to $j\omega$ is an inductor. The

analogous circuit is shown in Fig.. 6(b). For a tube of air to act as a pure acoustic mass, each particle of air in the tube must move with the same velocity. This is strictly true only if the frequency is low enough. Otherwise, the motion of the air particles must be modeled by a wave equation. An often used criterion that the air in the tube act as a pure acoustic mass is that its length must satisfy $l \le \lambda/8$, where λ is the wavelength.

Radiation impedance of a baffled rigid piston

Radiation impedance can be easily explained by an example of the diaphragm vibration. When the diaphragm is vibrating, the medium reacts against the motion of the diaphragm. The phenomenon of this can be described as there is impedance between the diaphragm and the medium. The impedance is called the radiation impedance.

The detail of the theory of radiation impedance is clearly described by Bernek. The analogous circuit of the radiation impedance for the piston mounted in an infinite baffle is shown in Fig. 7. The acoustical radiation impedance for a piston in an infinite baffle can be approximately over the whole frequency range by the analogous circuit. The parameters of the analogous values are given by

$$M_{A1} = \frac{8\rho_0}{3\pi^2 a} \tag{31}$$

$$R_{A1} = \frac{0.4410\rho_0 c}{\pi a^2} \tag{32}$$

$$R_{A2} = \frac{\rho_0 c}{\pi a^2} \tag{33}$$

$$C_{A1} = \frac{5.94a^3}{\rho_0 c^2} \tag{34}$$

where ρ_0 is the density of air, c is the sound speed in the air, a is the radius of the circuit piston.

Radiation impedance on a piston in a tube

The flat circuit piston in an infinite baffle that is analyzed in the preceding section is commonly used to model the diaphragm of a direct-radiator loudspeaker when the enclosure is installed in a wall or against a wall. If a loudspeaker is operated away from a wall, the acoustic impedance on its diaphragm changes. It is not possible to exactly model the acoustic radiation impedance of this case. An approximate model that is often used is the flat circuit piston in a tube.

The analogous circuit for the piston in a long tube is the same from as that for the piston in an infinite baffle; only the element values are different. The analogous circuit is given in Fig. 7. The parameters of the analogous values are given by

$$M_{A1} = \frac{0.6133\rho}{\pi a} \tag{35}$$

$$R_{A1} = \frac{0.5045\rho c}{\pi a^2} \tag{36}$$

$$R_{A2} = \frac{\rho c}{\pi a^2} \tag{37}$$

$$C_{A1} = \frac{0.55\pi^2 a^3}{\rho c^2} \tag{38}$$

Transmission line model of a duct

Consider a length of duct, we can write the pressure at any point in the duct as a superposition of two standing waves:

$$p(x) = B_1 \cos kx + B_2 \sin kx \tag{39}$$

(We could also have started with the superposition of two traveling waves, one in each direction.) Using this expression, we will evaluate the constants, $B1$ and $B2$, so that the pressure at $x = 0$ is $p1$ and the volume velocity at $x = 0$ is $U1$. Find $U(x)$ from Newton's second law in a fluid,

$$-\frac{dp}{dx} = j\omega\rho v \tag{40}$$

$$U(x) = -v \cdot A = \frac{A}{j\omega\rho}\frac{dp}{dx} \tag{41}$$

$$U(x) = \frac{Ak}{j\omega\rho}[-B_1 \sin kx + B_2 \cos kx] \tag{42}$$

Replace B_1 and B_2 by using the pressure and volume velocity at $x = 0$ and evaluate the pressure and volume velocity at $x = L$.

$$p_2 = p_1 \cos kL + U_1(\frac{j\omega\rho}{Ak} \sin Kl) \tag{43}$$

$$U_2 = p_1(-\frac{Ak}{j\omega\rho} \sin kL) + U_1 \cos kL \tag{44}$$

$$\begin{bmatrix} p_2 \\ U_2 \end{bmatrix} = \begin{bmatrix} \cos kL & -\frac{Ak}{j\omega\rho} \sin kL \\ \frac{j\omega\rho}{Ak} \sin kL & \cos kL \end{bmatrix} \begin{bmatrix} p_1 \\ U_1 \end{bmatrix} \tag{45}$$

These equations are in transfer matrix form.

Compare to transfer matrix for the T-circuit shown in Fig. 8. Its transfer matrix is shown below:

$$\text{T}=\begin{bmatrix} 1+\frac{Z_a}{Z_b} & Z_a\left(2+\frac{Z_a}{Z_b}\right) \\ \frac{1}{Z_b} & 1+\frac{Z_a}{Z_b} \end{bmatrix} \tag{46}$$

Then Z_a and Z_b can be got as:

$$Z_a = jZ_0 \tan(\frac{kL}{2})$$

$$Z_b = \frac{Z_0}{j \sin kL} \tag{47}$$

$$Z_0 \equiv \frac{\rho c}{A}$$

Other acoustic elements

Perforated sheets are often used as an acoustic resistance in application where an acoustic mass in series with the resistance is acceptable. Fig. 9(a) illustrates the geometry. If the holes in the sheet have centers tat are spaced more than on diameter apart and the radius a of the holes satisfies the inequality $0.01/\sqrt{f} < a < 10/f$, where f is the frequency and a is in m, the acoustic impedance of the sheet is

given by

$$Z_A = \frac{\rho_0}{N\pi a^2}\left\{\sqrt{2\omega u}\left[\frac{t}{a}+2\left(1-\frac{\pi a^2}{b^2}\right)\right]+j\omega\left[t+1.7\left(1-\frac{a}{b}\right)\right]\right\} \tag{48}$$

where N is the number of holes. The parameters μ is the kinematic coefficient of viscosity. For air at $20^{\circ}C$ and 0.76 mHg, $\mu \approx 1.56\times10^{-5}\ m^2/s$. This parameter value approximately as $T^{1.7}/P_0$, where T is the Kelvin temperature and P_0 is the atmospheric pressure.

A tube having a very small diameter is another example of an acoustic element which exhibits both a resistance and a mass. If the tube radius a in meters satisfies the inequality $a < 0.002/\sqrt{f}$, the acoustic impedance is given by

$$Z_A = \frac{8\eta l}{\pi a^4} + j\omega\frac{4\rho_0 l'}{3\pi a^2} \tag{49}$$

where l is the actual length of the tube and l' is the length including end corrections. The parameter η is the viscosity coefficient. For air, $\eta = 1.86\times10^{-5}\ N\cdot S/m^2$ at $20^{\circ}C$ and 0.76 mHg. This parameter varies with temperature as $T^{0.7}$, where T is the Kelvin temperature. If the radius of the tube satisfies the inequality $0.01/\sqrt{f} < a < 10/f$, the acoustic impedance is given by

$$Z_A = \frac{\rho_0}{\pi a^2}\sqrt{2\omega u}\left(\frac{l}{s}+2\right)+j\omega\frac{\rho_0 l'}{\pi a^2} \tag{50}$$

For a tube with a radius such that $0.002/\sqrt{f} < a < 0.01/\sqrt{f}$, interpolation must be used between the two equations.

A narrow slit also exhibits both acoustic resistance and mass. Fig. 9(b) shows the geometry of such a slit. If the height t of the slit in meters satisfies the inequality $t < 0.003/\sqrt{f}$, the acoustic impedance of the slit, neglecting end corrections for the mass term, is given by

$$Z_A = \frac{12\eta l}{t^3 \omega} + j\omega \frac{\rho_0 l}{5\omega t} \tag{51}$$

2.4 Formulation of the ESM

In this section, the ESM is used to calculate the pressure field of an omni-directional source. The pressure of a linear sound field can be represented by a simple layer potential [29]-[31] as

$$p(\mathbf{x}) = \int_S \sigma(\mathbf{y}) G(\mathbf{x}, \mathbf{y}) dS(\mathbf{y}), \tag{52}$$

where

$$G(\mathbf{x}, \mathbf{y}) = \frac{e^{-jkr}}{4\pi r} \tag{53}$$

being the free-space Green's function between the source point **x** and the field point **y**, $\sigma(\mathbf{y})$ is an unknown source strength of the point source distribution, j denotes $\sqrt{-1}$, $k = \omega / c$ is wave number, c is speed of sound, ω is angular frequency and $r = |\mathbf{x} - \mathbf{y}|$. The basic idea of ESM is to model sound field by using distribution of virtual simple sources, as shown in Fig. 10. The symbol $\mathbf{z}_m$ is the mth measured position on the free space surface S_f. The symbol $\boldsymbol{x}_l$ is the lth sampled point on the actual source surface S_s. The symbol $\boldsymbol{y}_i$ is the ith virtual source point on the virtual surface S_v.

The configuration used in this thesis is shown in Fig. 11, in the configuration, the virtual source surface S_v is kept away from the actual source surface S_s with a non-zero retreat distance. Due to singularity of virtual point sources, we need a non-zero retreat distance between the virtual source surface S_v and the actual source surface S_s to assure smooth computation results. The sound pressure on the actual source surface can be written by discretizing Equation (52)

$$p(\mathbf{x}_l)=\int_S \sigma(\mathbf{y})G(\mathbf{x},\mathbf{y})dS(\mathbf{y}) \approx \sum_{i=1}^{I}\int_{S_i} \sigma(\mathbf{y})G(\mathbf{x},\mathbf{y})dS(\mathbf{y})$$
$$\approx \sum_{i=1}^{I}\left[\sigma(\mathbf{y}_i)\hat{S}_i\right]G(\mathbf{x}_l,\mathbf{y}_i)=\sum_{i=1}^{I}a_i\frac{e^{-jkr_{li}}}{r_{li}} \quad , \qquad (54)$$

where I is the number of focal point, $\hat{S}_i$ is the area on the virtual source of the ith element, $y_i \in \hat{S}_i$, a_i represents the source amplitude of the ith point source and $r_{li}=|\mathbf{x}_l-\mathbf{y}_i|$. The particle velocity can be expressed via the momentum equation as

$$u(\mathbf{x}_l)=\frac{-1}{j\rho_0\omega}\frac{\partial}{\partial n}p(\mathbf{x})=\frac{1}{\rho_0 c}\sum_{i=1}^{I}(\mathbf{n}\bullet\mathbf{e}_{li})\left(1+\frac{1}{jkr_{li}}\right)\frac{a_i e^{-jkr_{li}}}{r_{li}}$$
$$=\sum_{i=1}^{I}d_i a_i \quad , \qquad (55)$$

where

$$d_i=\frac{1}{\rho_0 c}(\mathbf{n}\bullet\mathbf{e}_{li})\left(1+\frac{1}{jkr_{li}}\right)\frac{e^{-jkr_{li}}}{r_{li}} \qquad (56)$$

being the transfer function between the source point **x** and the field point **y**, $\mathbf{e}_{li}=(\mathbf{x}_l-\mathbf{y}_i)/|\mathbf{x}_l-\mathbf{y}_i|$ is the unit vector pointing from the ith virtual source to the lth actual source point and **n** is the outward unit normal vector. Equation (55) can be written into the matrix form

$$\mathbf{u}=\mathbf{D}\mathbf{a}, \qquad (57)$$

where **u** represents the velocity vector, **a** represents the virtual source amplitude vector, **D** is the transfer function matrix between virtual source points and actual source points. In this case, because of the velocity on the actual source is known so that the unknown source amplitude can be calculated by inverting Eq. (57).

$$\hat{\mathbf{a}}=\mathbf{D}^{+}\mathbf{u} \qquad (58)$$

where $\hat{\mathbf{a}}$ is the estimated source amplitude vector, $\mathbf{D}^{+}$ is the pseudo-inverse matrix from **D**. In practice, truncated singular value decomposition (TSVD) or Tikhonov regularization [32] can be used to deal with the ill-conditioned inversion process of calculated source amplitude.

3. Acoustical design of an Earphone

3.1 Electro-acoustic modeling of earphone

3.1.1 EMA analogous circuit of earphone

In this section, a lumped parameter model based on EMA analogy is established for the earphone. The cross-section of an earphone connected to the type 3.3 ear simulator and the experimental arrangement and the lumped parameter model are shown in Figs. 12 and 13, respectively. In Fig. 1(a), the coupling of the electrical and the mechanical domains is modeled by a gyrator, whereas the coupling of the mechanical and the acoustical domains is modeled by a transformer. The T-S parameters of the microspeaker identified via an electrical impedance measurement are summarized in Table 1. A distinct feature of the electroacoustic modeling of the earphone as compared with the other free-field loudspeaker systems is the ear canal impedance. To gain an appreciation of the main difference of these two environments, the ear canal is approximated as a cavity with acoustic compliance C_A. Simplifying the circuit in the acoustical domain leads to the pressure response at the ear canal

$$p_c = \left(\frac{\rho_0}{2\pi r}\right)\frac{C'Bl}{C_A S_D R_E}\frac{1}{\left(\frac{s}{\omega_s}\right)^2 + \left(\frac{1}{Q_{AT}}\right)\left(\frac{s}{\omega_s}\right)+1} e_g , \tag{59}$$

where ρ_0 is air density, r is distance from the microspeaker diaphragm to the measurement point. $C' = \frac{C_A C_{AS}}{C_A + C_{AS}}$, $\omega_s = \frac{1}{\sqrt{M_{AD} C'}}$, $Q_{AT} = \frac{1}{R_{AT}}\sqrt{\frac{M_{AD}}{C'}}$, C_{AS} is the acoustic compliance of the suspension, M_{AD} is the acoustic mass of the diaphragm, $R_{AT} = \frac{(Bl)^2}{S_D^2 R_E} + \frac{R_{MS}}{S_D^2}$, Bl is the force factor of the voice coil, R_E is the voice-coil resistance, R_{MS} is the mechanical resistance of the suspension, and S_D is

the effective area of the diaphragm. It should be noted that the equation above is valid only for the low-frequency pressure response. The multiplication factor $\frac{\rho_0}{2\pi r}$ could be omitted when compared to the pressure transfer function for direct radiation in the free-field conditions. It follows that the pressure response has a second-order low-pass characteristic, which is quite different from a direct radiator typically having a second-order high-pass characteristic. Note that, since the acoustic compliance C' is effectively decreased due to the ear canal impedance, the system quality factor Q_{AT} will be increased. Thus, it is crucial in designing earphones to "shape" the resonant peak at ω_s for an acceptable Q_{AT} value.

Apart from the approximation above, a more detailed circuit model of the acoustical system is illustrated in Fig. 14. The acoustical system primarily consists of three parts: a cavity (C_{AF}) and a duct in front of the speaker, the type 3.3 ear simulator, and a cavity (C_{AB}) with a leakage hole behind the speaker.

The duct in front of the speaker can be modeled as an acoustic resistance [9] R_{ST} cascaded with a transmission line which can be simulated with a T-circuit with parameters Z_{STA} and Z_{STB}. The T- circuit with parameters is given by

$$Z_A = jZ_0 \tan(\frac{kL}{2}) \tag{60}$$

$$Z_B = \frac{Z_0}{j \sin kL} \tag{61}$$

$$Z_0 = \frac{\rho_0 c}{\pi a^2}, \tag{62}$$

where $Z_{STA} = Z_A$, $Z_{STB} = Z_B$, $a = a_{ST}$ is the radius of the cross-section of the duct, $L = L_{ST}$ is the length of the duct, and $k = \frac{\omega}{c}$ is the wave number.

The analogous circuit of the type3.3 ear simulator using IEC 60711 ear simulator [33]-[34] is shown in Fig. 14. The equivalent circuit of the type 3.3 simulator models the low-leak simplified pinna simulator and the ear simulator [15], as shown

in Figs. 15 and 16, respectively. In the electrical equivalent circuit of the IEC 60711 coupler in Fig. 16, the LC components corresponding to M_{A4}, C_{A4}, M_{A6} C_{A6}, M_{A8} and C_{A8} represent the ear canal that is approximated by a tube of rigid walls with constant cross section. The two RLC circuits with components R_{A5}, M_{A5}, C_{A5}, R_{A7}, M_{A7} and C_{A7} are used to match the eardrum impedance[35]. The acoustic parameters of the type 3.3 ear simulator are summarized in Table 2.

The leakage hole impedance is given in the acoustical domain as [9]

$$Z_{LK} = R_{LK} + j\omega M_{LK} \tag{63}$$

The leakage hole can cause the radiation by air loading. The acoustic element parameters calculated according to the formulas given in [9] in Sections 3.7 and 3.8 are summarized in Table 2. This analogous circuit serves as the simulation platform for the earphone.

3.1.2 Verification of the lumped parameter model

The volume velocity U_{AE} flowing through C_{A8} in the ear simulator can be obtained from solving the analogous circuit in Fig.2. From U_{AE}, the pressure p_{CA8} at the element C_{A8} can be calculated by

$$p_{CA8} = U_{AE} \frac{1}{j\omega C_{A8}} \tag{64}$$

Therefore, the sound pressure at tympanic membrane position p_{ED} is given by

$$p_{ED} = p_{CA8}, \tag{65}$$

The arrangement of experiment according to the ITU-T p.57 standard [15] is shown in Fig. 14. Experiments were undertaken to validate the aforementioned earphone simulation model. It can be observed from Fig. 17 that the Sound Pressure Level (SPL) response predicted by lumped parameter model (blue line) is in good agreement with the measurement (red line).

3.2 Optimization of the enclosure design of earphone

The SPL response of the earphone shown in Fig. 17 did not meet the requirement in 3GPP2 C.S0056-0 [13]. The peak at 2 kHz exceeded the frequency response mask. This calls for optimization of the enclosure design, where Simulated annealing (SA) [36] is exploited in this study.

SA is a generic probabilistic meta-algorithm for the global optimization problem, namely, locating a good approximation to the global optimum of a given function in a large search space [37]. SA's major advantage over other methods is the ability to avoid becoming trapped at local minima [38]-[39]. The algorithm employs a random search which, in the initial stage, not only accepts changes that decrease the cost function Q but also changes (bad solutions) that increase it. The acceptance of the bad solutions is determined by the probability

$$P = \exp\left(-\frac{\Delta Q}{T}\right) > \gamma(0,1), \tag{66}$$

where ΔQ is the increase in Q and T is a control parameter, which by analogy is known as the system "temperature" irrespective of the cost function involved. $\gamma(0,1)$ is a random number generated uniformly in the interval (0,1).

In the earphone optimization, we choose the initial temperature $T_i = 200$ and the final temperature $T_f = 10^{-3}$. The temperature decrement rule is given by

$$T_{k+1} = \alpha T_k, \tag{67}$$

where the annealing coefficient $\alpha = 0.95$ when $T > 20$, $\alpha = 0.99$ when $T < 20$. The solution will be rejected if it fails to comply with the the frequency response mask. The cost function for the SA optimization is chosen to be

$$Q = \sum_{n=1}^{95} \left[SPL_{new}(n) - L_{ref}(n) \right]^2 , \tag{68}$$

where SPL_{new} is the SPL of the current design, while L_{ref} is a smooth reference SPL curve passing the central region of the mask. The parameter n is the frequency index within the band 20–4500 Hz. The frequency range from 20 to 4500 Hz is sufficient for human speech application [40]. In each iteration of the optimization procedure, random numbers are generated within the constraint intervals to perturb the current design parameters. The design variables and the associated constraints are given in the following inequalities:

$$\begin{cases} 5\times10^{-4} \le a_{SP} \le 1.2\times10^{-2} \\ 10^{-3} \le L_{SP} \le 1.5\times10^{-2} \\ 3\times10^{-8} \le V_{AF} \le 5\times10^{-7} \\ 3\times10^{-8} \le V_{AB} \le 3\times10^{-7} \end{cases}, \tag{69}$$

where a_{SP} is the radius of the duct, L_{SP} is the length of the duct, V_{AF} is the volume of the front cavity, and V_{AB} is the volume of the back cavity.

With the SA procedure, the optimized enclosure parameters are compared with the original non-optimized ones in Table 3. Note that the radius of duct has the largest design change to make. The port legth has to be added to 375% of its original size. The SPL responses of the optimal and original designs are compared in simulation and experiment, as shown in Fig. 18. As opposed to the original non-optimized design, the optimized design effectively lowers the resonance peak to be within the frequency response mask of 3GPP2.

4. The source design by using ESM model

4.1 The structure design of omni-directional source

In this thesis, the structure of omni-directional source is selected as a dodecahedron which is mounted a moving-coil speaker on every surface. The mesh configuration of the source is created by Soildworks 2007® triangular mesh code. The perspective drawing of three surfaces is shown in Fig. 19. All of the dimensional parameters about this ESM model are summarized in Table 4. On the actual source surface, red line and black line are indicated the actual source position and fixed boundary position, respectively. The discrete points of dodecahedron source are shown in Fig. 20, red points and black points are meant the actual source and fixed boundary, respectively. The given initial velocity on red line and black line are u = 5m/s and u = 0m/s, respectively. The blue and green dotted line are meant the virtual source surface and free field surface, respectively. The virtual source surface is shrunk as a conformal dodecahedron. The inner circle radius of virtual source surface R_b is shorter than actual source R_a. The free space surface is the discrete sphere points with a radius R_c. The origin is set on the center of inner circle of dodecahedron source. The numbers of discrete points on three surfaces are also summarized in Table 4.

In order to calculate the retreat distance, the average lattice spacing had to be determined. The total area A of the dodecahedron source is 0.2065 m^2, every discrete point has a average area 7.12×10^{-4} m^2 on dodecahedron source. In this case, the average area of every discrete point is regarded as a square, therefore, the lattice spacing d can be calculated as square root of average area is 2.67×10^{-2} m. Therefore, the retreated distance r_t can be regarded as one time lattice spacing [32], [41]-[42] is 2.67×10^{-2} m. The maximum frequency has been calculated by following the $\lambda/2$

rule [42]-[43] is 6.5 kHz.

4.2 Establishing the ESM model

In this thesis, the dodecahedron is selected to be the structure of omni-directional source. There are twelve regular pentagonal surfaces to form a regular dodecahedron surface. Therefore, to make a regular pentagon which is mounted a speaker is the first step of designing this omni-directional source. The length of regular pentagon sides is *L* and the depth of regular pentagon is *D*. A moving-coil speaker has been mounted at the center of regular pentagon and the material of pentagon is stainless steel.

Combining those twelve regular pentagons to form a regular dodecahedron is the final step. The dihedral angle of regular dodecahedron is $\theta = \cos^{-1}\left(-1/\sqrt{5}\right)$. Welding twelve pentagons to form the dodecahedral speaker according to the geometric structure and dihedral angle and the finished work is shown in Fig. 21.

4.3 Experimental investigation

Experiments were undertaken to validate the aforementioned ESM model and omni-directional speaker. The dodecahedral speaker was placed on a turn table and the distance between microphone and the origin is 1m on horizontal surface of dodecahedral speaker. The sound pressure is measured by every 5 degrees from 0 degree to 360 degrees. The sound pressure response of simulation and experiment are compared with polar plots as shown in Figs. 22-25. Fig. 22 represents the frequency response on 1 kHz, Fig. 23 represents the frequency response on 3.15 kHz, Fig. 24 represents the frequency response on 8 kHz and Fig. 24 represents the frequency response on 14 kHz. Those four frequencies are chosen from low to high

frequency according to the analyzer setting frequencies. It can be observed from Figs. 22-25 that the sound pressure directivity predicted by ESM model (dotted line) is in good agreement with the measurement (solid line) even in high frequency. Besides, it is also shown in Figs. 22-25 that there is no obvious directivity on the polar plots from low to high frequency. Although the speaker is not a perfectly omni-directional source, the performance is deemed sufficient in real application.

5. Conclusions

Earphones are faced with ear canal impedance, which is fundamentally different from direct radiator loudspeakers exposed in a free-field environment. EMA analogous circuits have been developed to model the earphone. On the basis of this simulation model, the enclosure design of the earphone has been optimized using the SA technique. The SPL response resulting from the optimized design has been significantly enhanced and the 3GPP2 standard has been met.

Comparing to the other methods (BEM, FEM), the use of the ESM is not restricted to source with regular geometries which can model the source with any kind of structures. Although the structure used in this paper is dodecahedral speaker, all modeling approaches in the paper can be generalized to any type of speaker structures. The simulated and experimental results are shown that ESM model can provide sufficient accuracy to model this dodecahedral speaker. The sound pressure directivity resulting from the dodecahedral speaker is approximated to omni-directional source. Although sound pressure of this dodecahedral speaker is not the same at every direction to match a perfect omni-directional source but the performance is deemed sufficient in real application.

6. APPENDIX

Finite Element Analysis of the Voice coil system Assembly

In contrast to large loudspeakers, the structures of micro-speakers are generally simplified enough with suspension removed. The diaphragm serves as not only a sound radiator but also the suspension. Thus, the pattern design of the diaphragm is crucial to the overall response and performance of a micro-speaker. In another hand, the magnetic constant usually is measured by T-S parameter identification. In this thesis, a hybrid approach that combines finite element analysis (FEA) and electro-mechano- acoustical (EMA) analogous circuit is presented to provide a more accurate model than the conventional approaches. And the magnetic constant has been designed also by using FEA analysis. Compared to traditional micro-speaker design, this new hybrid method can predict frequency response without producing product.

I. Finite Element Analysis of the Magnetic System

In this thesis, the micro-speaker is used type: DMS1608F-02-G as shown in Fig. 26(a)-(b). The FEA is applied to model the magnetic system assembly shown in Figs. 27(a)-(b) with dimensions summarized in Table 5. The FEA is conducted using FEMLAB3.1® [44]. The boundary conditions are selected as non-conductivity. The magnet is the type N38 that is the commonly synthesized magnet (NeFeB). The input voltage V_{input} is 0.5V. The magnetic flux density (B) can be measured as shown in Fig. 28. The effective length l of the wire which cuts the magnetic field is shown in Fig. 29. The parameter n_m is the number of times that the wire circled magnet. The average magnetic flux density has been calculated by averaging red and green line as shown in Fig. 30. The average B_{red} and B_{green} are 7.5093(T) and 8.2134 (T), respectively. Therefore, the parameter Bl has been calculated as a

average value Bl=0.4578(T-m). The Bl measured by T-S parameter identification is 0.441(T-m). The difference between FEA model and T-S parameter is 3.8% error that shows proper accuracy result by using FEA model.

II. Finite Element Analysis of the Diaphragm-Voice coil Assembly

The material properties of the diaphragm-voice coil assembly are included in Table 6. The FEA is conducted using ANSYS® [45], where the element "shell 63" is used. The shell element has four nodes and 6 degrees of freedom (U_x, U_y, U_z, ROT_x, ROT_y, ROT_z) at each node. The finite element model and the mesh of the diaphragm with voice-coil are shown in Figs. 31 (a)-(b). The boundary conditions are selected that all degrees of freedom for the outer rim of the diaphragm and the X, Y-displacements of the voice-coil are set to zero. The fundamental resonance frequency calculated by the modal analysis is 811.68 Hz and the associated mode shape is shown in Fig. 32 (a). The fundamental mode known as the piston mode can be used to "fine-tune" FEA parameters to match the measured data. The measured result of the fundamental resonance frequency is 856.98 Hz which is about 5.28% higher than the FEA prediction. Figure 32 (b) shows another higher order mode at 17568 Hz, where major motion takes place at the center circular portion inside the voice-coil bobbing, while the outer ring of the diaphragm is almost motionless. Due to this nature, we call it the second piston mode. The SPL response shows a peculiar boost above the second piston mode, as will be seen in the experimental results. In order to fit the aforementioned FEA model into the analogous circuit of the microspeaker system, the dynamics of the FEA model has to be adapted into a lumped parameter model next. To begin with, the short-circuit mechanical impedance (Z_{ms}) defined in the following expression is calculated using the FEA harmonic analysis:

$$Z_{ms} = \frac{f}{\bar{u}}, \tag{70}$$

where $\bar{u}$ denotes the mean velocity of the diaphragm and f is the excitation force delivered by the voice-coil unit.

$$f = Bli \tag{71}$$

$$i = \frac{V_{input}}{R_e} \tag{72}$$

According the above measured parameter, the excitation force can be calculated as 0.03 N. The damping ratio is assumed to be 0.16 and 0.07 for 20 ~ 4000 Hz and for 4k ~ 20 kHz, respectively. The complex displacements calculated using the FEA harmonic analysis are then converted into the average velocity ($\bar{u}$). Using Eq. (70), the mechanical impedance of the diaphragm-voice coil assembly Z_{ms} can be calculated, as shown in Fig. 33. As a result, the dynamics of the flexible diaphragm is represented by a frequency-dependent impedance element and is readily integrated into the analogous circuit.

REFERENCES

[1] I. Chun, P. A. Nelson and J. T. Kim, “Numerical models of miniature loudspeakers,” in *The 32nd International Congress and Exposition on Noise Control Engineering*, Jeju Island, Korea, Aug. 2003.

[2] S. J. Oh, H. R. Lee, S. W. Yoon and J. S. Park, “Study of the Acoustical Properties as a Function of Back Cavity for Loudspeaker,” in *The 32nd International Congress and Exposition on Noise Control Engineering*, Jeju Island, Korea, Aug. 2003.

[3] C. H. Choi, H. S. Yoon, “Acoustic and Vibration Characteristics of a Micro Speaker through the Electro-Magnetic field Analysis,” in *The 32nd International Congress and Exposition on Noise Control Engineering*, Jeju Island, Korea, Aug. 2003.

[4] S. H. Lee, J. H. Kim, J. T. Kim, O. S. Kwon and C. H. Choi, “Development of the simulation program to analyze acoustic characteristics of a miniature type loudspeaker,” in *The 32nd International Congress and Exposition on Noise Control Engineering*, Jeju Island, Korea, Aug. 2003.

[5] A. Bright, “Simplified Loudspeaker Distortion Compensation by DSP,” in *The 23rd AES International Conference*, Copenhagen, Denmark, May 2003.

[6] M. R. Bai and R. L. Chen, “Optimal Design of Loudspeaker Systems Based on Sequential Quadratic Programming (SQP),” *J. Audio Eng. Soc.*, Vol. 55, No. 1/2, pp. 44-54, 2007.

[7] H. Olson, *Acoustical Engineering*, Van Nostrand, New York, 1957. Reprinted by Professional Audio Journals, Philadelphia, PA, 1991.

[8] L. L. Beranek, *Acoustics*, Acoustical Society of America, Woodbury, NY. 1996.

[9] W. M. Leach, Jr., *Introduction to Electroacoustics and Audio Amplifier Design*, Kendall-Hunt, Dubuque, IA, 2003.

[10] N. Thiele and R. Small, in *AES Loudspeaker Anthologies*, Vols. 1–3, Audio Engineering Society, New York, 1978, 1984, 1996.

[11] M. R. Bai and J., Liao, "Acoustic Analysis and Design of Miniature Loudspeakers for Mobile Phones," *Audio Engineering Society*, Vol. 53, No. 11, pp. 1061-1076, 2005.

[12] L. Ingber, "Simulated annealing: practice versus theory," *Mathematical and Computer Modelling* **18**, 11, 29-57 (1993).

[13] 3GPP2 C.S0056-0, "Electro-Acoustic Recommended Minimum Performance Specification for cdma2000 Mobile Stations," 3rd Generation Partnership Project 2, in annex C.1 and C4.2 (2005).

[14] IEC 60711, "Occluded-ear simulators for the measurement of earphones coupled to the ear by ear inserts," International Electrotechnical Commission, (1981).

[15] ITU-T Recommendation P.57, "Artificial ear," International Telecommunication Union, (2006).

[16] S. Linkwitz, "Investigation of Sound Quality Differences between Monopolar and Dipolar Woofers in Small Rooms," 105th AES Convention, San Francisco (1998).

[17] P. M. Hofman, "Relearning sound localization with new ears (PDF)." Nature Neuroscience **1** (5): 417–421(1998).

[18] M. Ochmann, "The source simulation technique for acoustic radiation problems," Acustica. **81**, 512–527 (1995).

[19] I.Y. Jeon and J.G. Ih, "On the holographic reconstruction of vibroacoustic fields using equivalent sources and inverse boundary element method," J. Acoust. Soc. Am.**118**, 3475–3484 (2005).

[20] A. Sarkissian, "Extension of measurement surface in near-field acoustic holography," J. Acoust. Soc . Am. **115**, 1593–1596 (2004).

[21] A. Sarkissian, “Method of superposition applied to patch near-field acoustic holography,” J. Acoust. Soc. Am. **118**, 671–678 (2005).

[22] G. H. Koopmann, L. Song, and J. B. Fahnline, “A method for computing acoustic fields based on the principle of wave superposition”, J. Acoust. Soc. Am. **86**, 2433-2438 (1989).

[23] L. Song, G. H. Koopmann, and J. B. Fahnline, “Numerical errors associated with the method of superposition for computing acoustic fields,” J. Acoust. Soc. Am., **89**, 2626-2633 (1991).

[24] J. B. Fahnline and G. H. Koopmann, “A numerical solution for the general radiation problem based on the combined methods of superposition and singular-value decomposition,” J. Acoust. Soc. Am. **90**, 2808–2819 (1991).

[25] Z. Zhang, N. Vlahopoulos, S. T. Raveendra, T. Allen, and K. Y. Zhang, ‘‘A computational acoustic field reconstruction process based on an indirect boundary element formulation,’’ J. Acoust. Soc. Am. **108**, 2167–2178 (2000).

[26] Z. Zhang, N. Vlahopoulos, T. Allen, and K. Y. Zhang, ‘‘A source reconstruction process based on an indirect variational boundary element formulation,’’ Eng. Anal. Boundary Elem. **25**, 93–114 (2001).

[27] R. Yang and X. W. Fan, “Finite/infinite element method for the acoustic radiating problem,” IEEE, Direct and Inverse Problems of Electromagnetic and Acoustic Wave Theory, 131 - 134 (2004).

[28] A. N. Thiele, “Loudspeakers in Vented-boxes: Part II,” *Audio Engineering Society*,Vol. 19, No. 6, pp. 471-483 (1971).

[29] G. H. Koopmann, L. Song, and J. B. Fahnline, “A method for computing acoustic fields based on the principle of wave superposition”, J. Acoust. Soc. Am. **86**, 2433-2438 (1989).

[30] L. Song, G. H. Koopmann, and J. B. Fahnline, “Numerical errors associated with

the method of superposition for computing acoustic fields," J. Acoust. Soc. Am., **89**, 2626-2633 (1991).

[31] J. B. Fahnline and G. H. Koopmann, "A numerical solution for the general radiation problem based on the combined methods of superposition and singular-value decomposition," J. Acoust. Soc. Am. **90**, 2808–2819 (1991).

[32] J. Gomes, J. Hald, P. Juhl and F. Jacobsen, 2009, "On the Applicability of the Spherical Wave Expansion with a Single Origin for Near-Field Acoustical Holography," J. Acoust. Soc. Am. **125,** 1529-1537 (2009).

[33] ITU-T Recommendation P.380, "Electroacoustic measurements on headsets," International Telecommunication Union, (2003).

[34] IEEE Standard 269-2002, "Standard Method for Measuring Transmission Performance of Analog and Digital Telephone Set, Handsets and Headset," (2009).

[35] S. Jønsson, B. Liu, A. Schumacher and L. Nielsen, "Simulation of the IEC 60711 occluded ear simulator," Proc. of the 116th Convention of the Audio Engineering Society, Berlin, May, (2004).

[36] O. de. Weck and C. Jilla, "Simulated Annealing: A Basic Introduction, Massachusetts Institute of Technology," http://ocw.mit.edu/NR/rdonlyres/Aeronautics-and-Astronautics/16-888Spring-2004/5F6CFF91-524F-4792-859D-98331A73AC7C/0/l10a_sa.pdf

[37] Y. P. Panos and J. W. Douglass, "Principles of Optimal Design : Modeling and Computation," Cambridge University Press, (2000).

[38] C. Enrico, C. Gianfranco and R. Emiliano, "Comparing deterministic and simulated annealing-based algorithms for minimum losses reconfiguration of large distribution systems", IEEE Bologna Power Tech Conference, Bologna, page7. Vol.2, June, (2003).

[39] Y. Maqsood, B. Ronald, K. A. Marc, L. Mark and L. A. Adriaan, “Simulated Annealing in pharmacokinetic modeling of PET neuroreceptor studies: accuracy and precision compared with other optimization algorithms”, Nuclear Science Symposium Conference Record, IEEE, page.3222 - 3225 Vol. 5, October, (2004).

[40] K. Kryter, “Effects of Noise on Men,” Academic Press, (1980)

[41] A. Sarkissian, “Method of superposition applied to patch near-field acoustic holography,” J. Acoust. Soc. Am. **118**, 671–678 (2005).

[42] N. P. Valdivia and E. G. Williams, “Study of the comparison of the methods of equivalent sources and boundary element methods for near-field acoustic holography,” J. Acoust. Soc. Am. **120,** 3694-3705 (2006).

[43] M. E. V. Pinho and J. R. F. Arruda, “On the Use of the Equivalent Source Method for Nearfield Acoustic Holography,” *ABCM Symposium Series in Mechatronics*. **1**, 590-599 (2004).

[44] 黃錦煌, 吳佐群, *輕鬆易學FEMLAB有限元素分析大師*(高立圖書, 台北市, 2004)

[45] Swanson Analysis Systems, ANSYS User’s Manual, Philadelphia, PA, 2005.

Table 1 Experimentally identified lumped-parameters of the microspeaker.

$R_E\,(\text{ohm})$	36.34	Q_{TS}	0.3192
$R_E^{/}\,(\text{m}^2)$	21.01	Q_{ES}	1.99306
$L_E\,(\text{mH})$	6.664×10^{-5}	Q_{MS}	0.38
$S_D\,(\text{m}^2)$	1.32×10^{-4}	$Bl\,(\text{T}\cdot\text{m})$	0.62
$F_S\,(\text{Hz})$	155.031	$V_{AS}\,(\text{L})$	0.04389

Table 2 The dimensions of the earphone and the parameters of acoustic analogous circuit.

Parameter	Value	Parameter	Value	Parameter	Value	Parameter	Value
$R_{ST}(Pa\times S/m^3)$	2.269×10^{6}	a_{ST} (m)	3.8×10^{-3}	$M_{A1}(kg/m^4)$	982.2	$C_{A2}(m^5/N)$	32.5×10^{-12}
$R_{LK}(Pa\times S/m^3)$	1.253×10^{5}	L_{ST} (m)	9×10^{-3}	$M_{A2}(kg/m^4)$	38.5	$C_{A3}(m^5/N)$	3.1×10^{-12}
$M_{LK}(kg/m^4)$	953.5	a_{EC} (m)	1.7×10^{-2}	$M_{A3}(kg/m^4)$	271.6	$C_{A4}(m^5/N)$	9×10^{-13}
$R_A(Pa\times S/m^3)$	6×10^{8}	L_{EC} (m)	1.66×10^{-2}	$M_{A4}(kg/m^4)$	78.8	$C_{A5}(m^5/N)$	1.9×10^{-12}
$M_A(kg/m^4)$	485.69	a_{AE} (m)	6×10^{-3}	$M_{A5}(kg/m^4)$	9.4×10^{3}	$C_{A6}(m^5/N)$	1.5×10^{-12}
$C_{AF}(m^5/N)$	7.653×10^{-10}	L_{AE} (m)	2×10^{-3}	$M_{A6}(kg/m^4)$	132.3	$C_{A7}(m^5/N)$	2.1×10^{-12}
$C_{AB}(m^5/N)$	4.278×10^{-12}			$M_{A7}(kg/m^4)$	983.8	$C_{A8}(m^5/N)$	2.1×10^{-12}
$R_{A1}(Pa\times S/m^3)$	1.7×10^{6}	$R_{A2}(Pa\times S/m^3)$	250×10^{3}	$M_{A8}(kg/m^4)$	153.5		
$R_{A5}(Pa\times S/m^3)$	5.06×10^{7}	$R_{A7}(Pa\times S/m^3)$	3.11×10^{7}				

Table 3 Parameters of the optimized design versus the original non-optimized design.

	Original design(1)	Optimal design(2)	(2)/(1) %
$a_{ST}\,(\mathrm{m})$	2×10^{-3}	2.3×10^{-3}	115%
$V_{AF}\,(\mathrm{m}^3)$	1.42×10^{-7}	2.12×10^{-7}	64.25%
$L_{ST}\,(\mathrm{m})$	9×10^{-3}	2.4×10^{-3}	375%
$V_{AB}\,(\mathrm{m}^3)$	6.14×10^{-8}	6×10^{-8}	102.33%

Table 4 The design parameters of the dodecahedral speaker

Parameters	Value	Parameters	Value
$R_a(m)$	0.0843	m	290
$R_b(m)$	0.111	i	290
$R_c(m)$	1	l	304
$r_t(m)$	0.0267	θ	$\cos^{-1}\left(-1/\sqrt{5}\right)$
$u(m/s)$	5	$u_0(m/s)$	0
$A(m^2)$	0.2065	$D(\mathrm{m})$	0.08
$d(\mathrm{m})$	0.0267	$L(\mathrm{m})$	0.1

Table 5. Experimentally identified lumped-parameters of a microspeaker

parameters	value	parameters	value
f_0 (Hz)	856.98	L_e (H)	$1.59e^{-5}$
R_E (ohm)	7.26	C_{AS} (m^5/N)	$1.45e^{-11}$
R_{ES} (ohm)	9.737	M_{AS} (kg/m^4)	2334.95
Q_{MS}	5.687	R_{AS} (ohm)	$2.21e^{6}$
Q_{ES}	4.241	C_{MES} (F)	$1.085e^{-4}$
Q_{TS}	2.429	L_{CES} (mH)	$3.180e^{-4}$
V_{AS} (L)	$2.103e^{-3}$	R_{AT} (ohm)	$5.18e^{6}$
C_{MS} (mm/N)	$1.637e^{-3}$	R_{MT} (ohm)	0.0467
M_{MS} (kg)	$2.11e^{-5}$	M_{MD} (kg)	$2.03e^{-5}$
R_{MS} (ohm)	0.01995	S_D (m^2)	$9.5e^{-5}$
Bl (T.m)	0.441	R_E' (m^2)	4.390

Table6. The dimensions of the diaphragm and voice-coil assembly of the microspeaker

Parameters	Value
Radius of diaphragm, *R*	**6.7 mm**
Thickness of diaphragm, *t*	**0.028 mm**
Height of inner arc, *H*	**0.5 mm**
Height of outer arc, *h*	**0.4 mm**
Bandwidth of outer arc, *d*	**2.8 mm**
Height of voice-coil, h_{vc}	**10 mm**

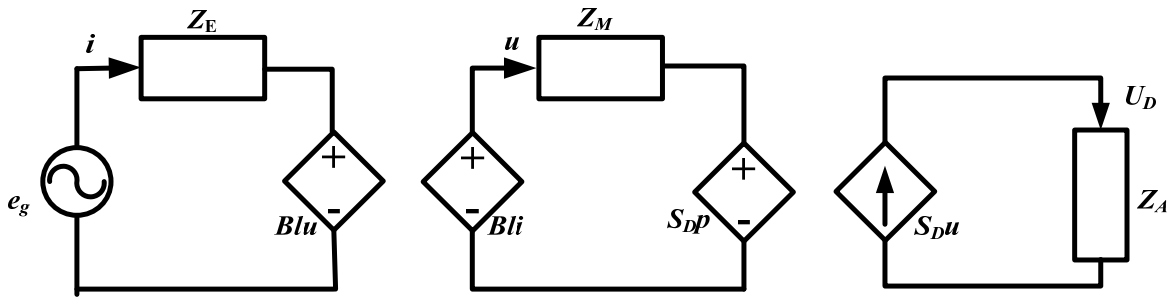

(a)

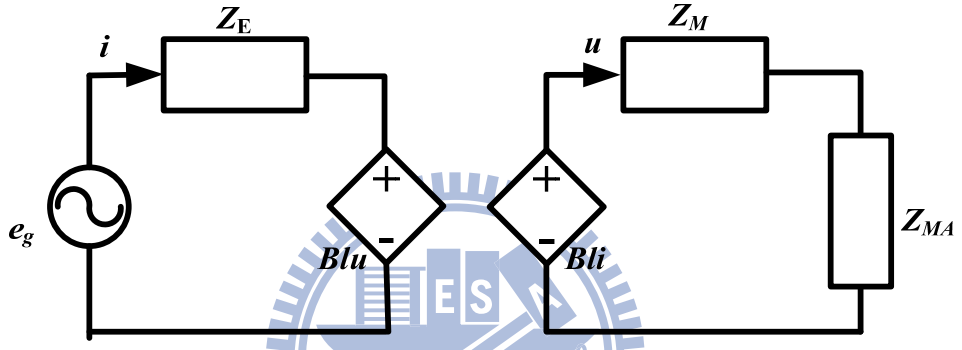

(b)

Figure 1 (a) Electro-mechano-acoustical analogous circuit of loudspeaker.

(b) Same circuit with acoustical impedance reflecting to mechanical system.

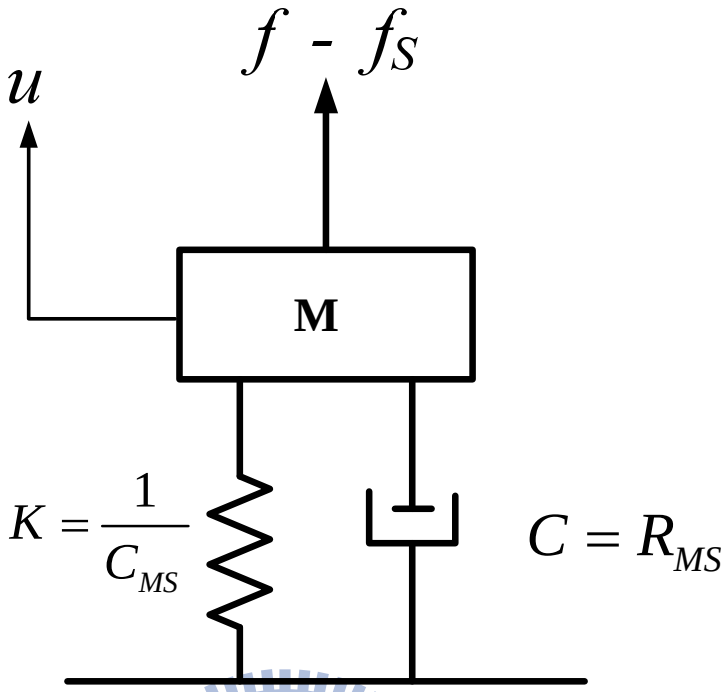

Figure 2 The mechanical system of loudspeaker. (M is diaphragm and voice coil mass, k is stiffness of suspension, C is damping factor)

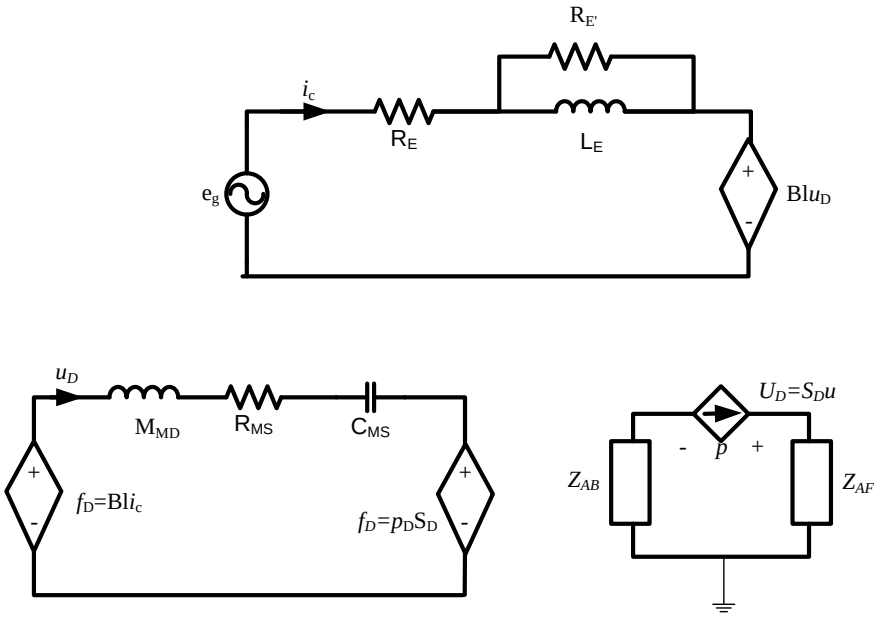

(a)

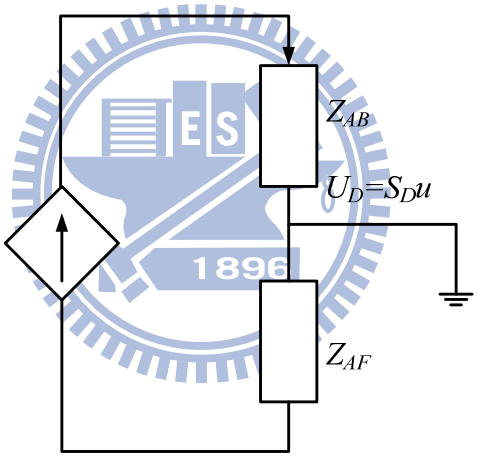

(b)

Figure 3 (a) Detailed Electro-mechanical-acoustical analogous circuit of loudspeaker.
(b) Another form of acoustic system.

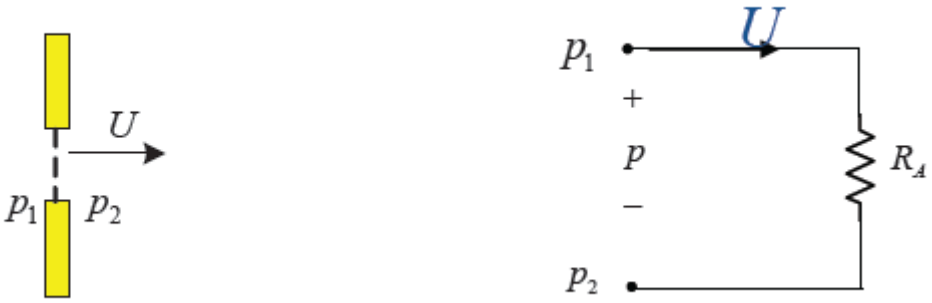

(a) (b)

Figure 4 (a) An acoustic resistance consisting of a fine mesh screen.
(b) Analogous circuit.

Figure 5 (a) Closed volume of air that acts as acoustic compliance.
(b) Analogous circuit.

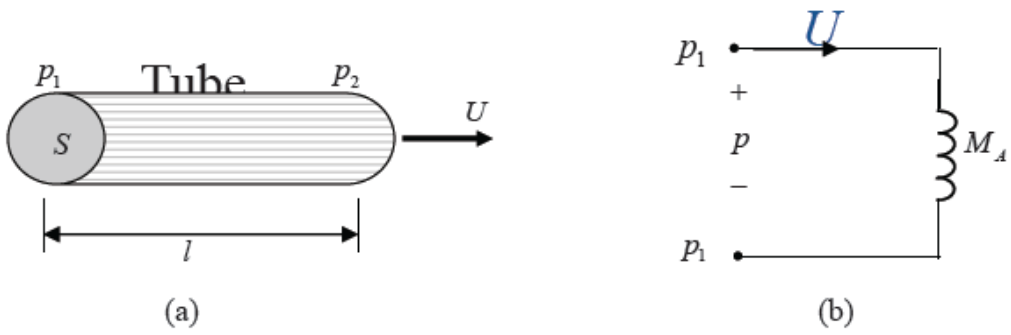

Figure 6 (a) Cylindrical tube of air which behaves as acoustic mass.
(b) Analogous circuit.

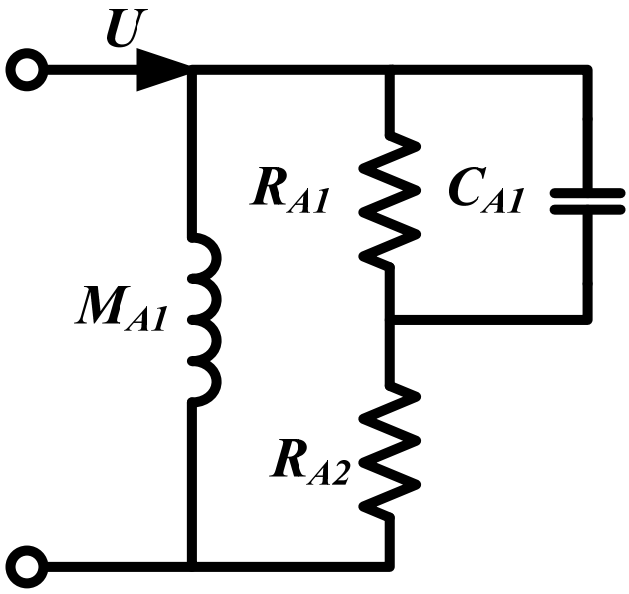

Figure 7 Analogous circuit for radiation impedance on a piston in a infinite baffle. Analogous circuit for radiation impedance on a piston in a tube.

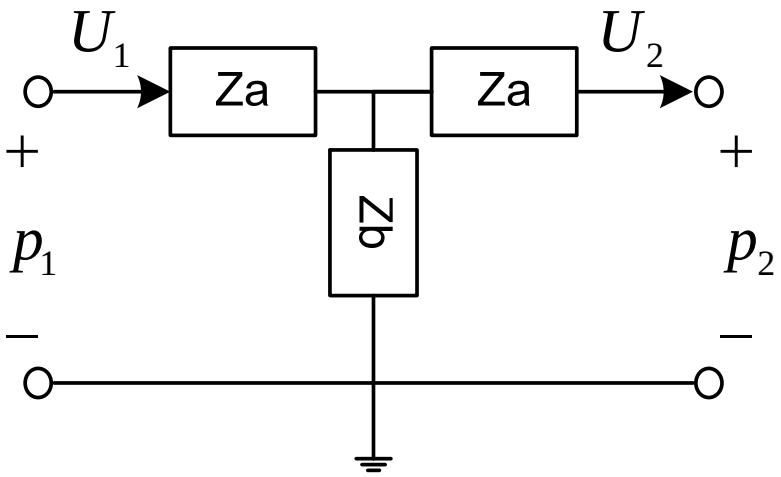

Figure 8 T-circuit of transmission line

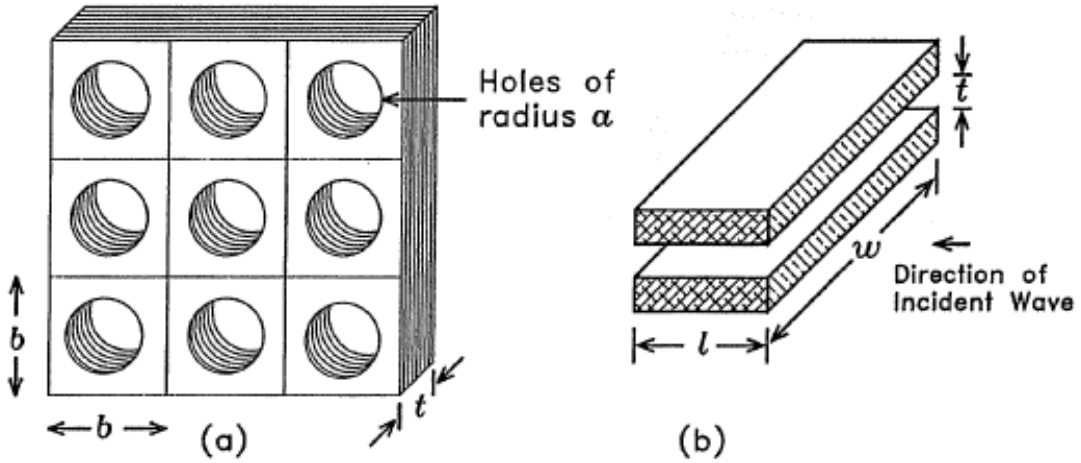

Figure 9 (a) Perforated sheet of thickness t having holes of radius a spaced a distance
(b) Geometry of the narrow slit.

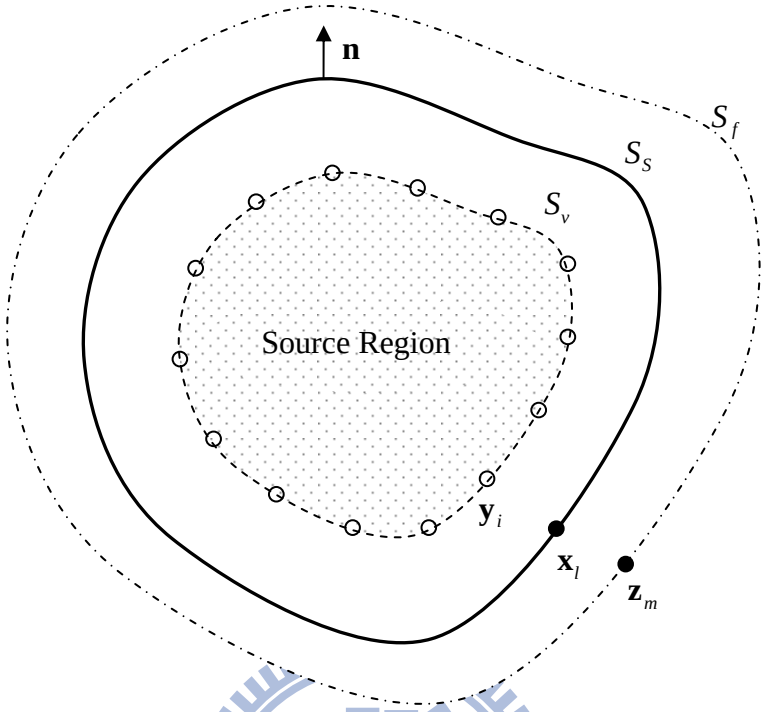

Figure 10 The definitions of important surfaces used in the ESM. The symbol $\mathbf{z}_m$ is the mth measured position on the free space surface S_f. The symbol $\boldsymbol{x}_l$ is the lth sampled point on the actual source surface S_s. The symbol $\boldsymbol{y}_i$ is the ith virtual source point on the virtual surface S_v.

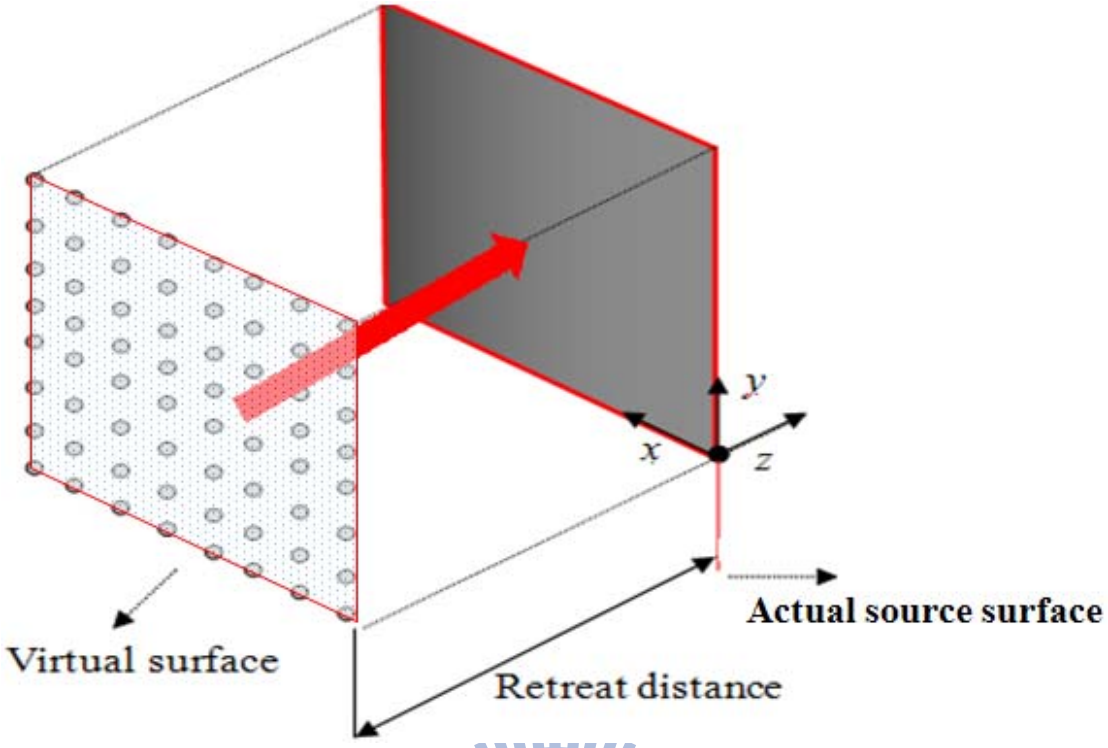

Figure 11 The configuration of ESM model

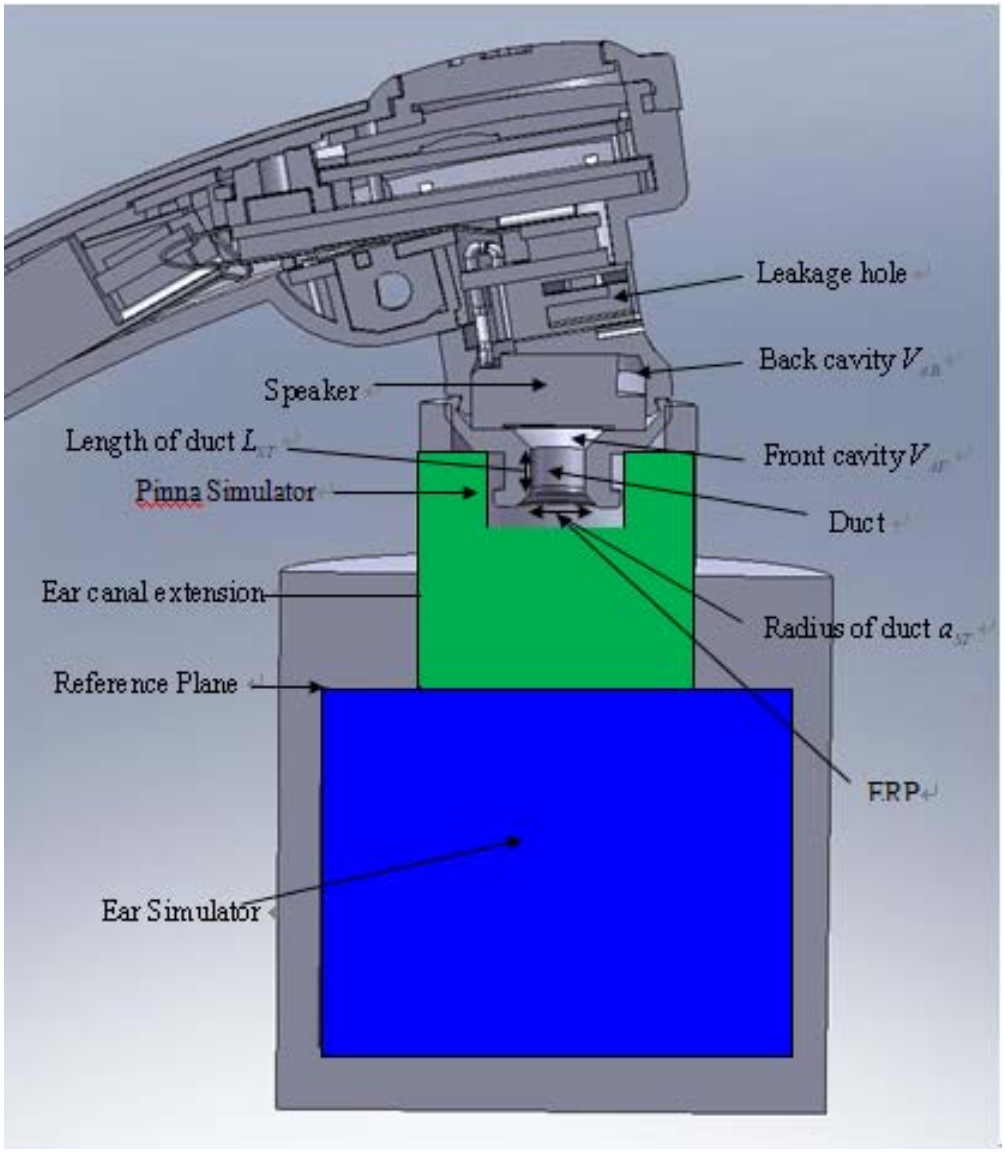

Figure 12 The cross-section of the earphone connected with the type 3.3 ear simulator.

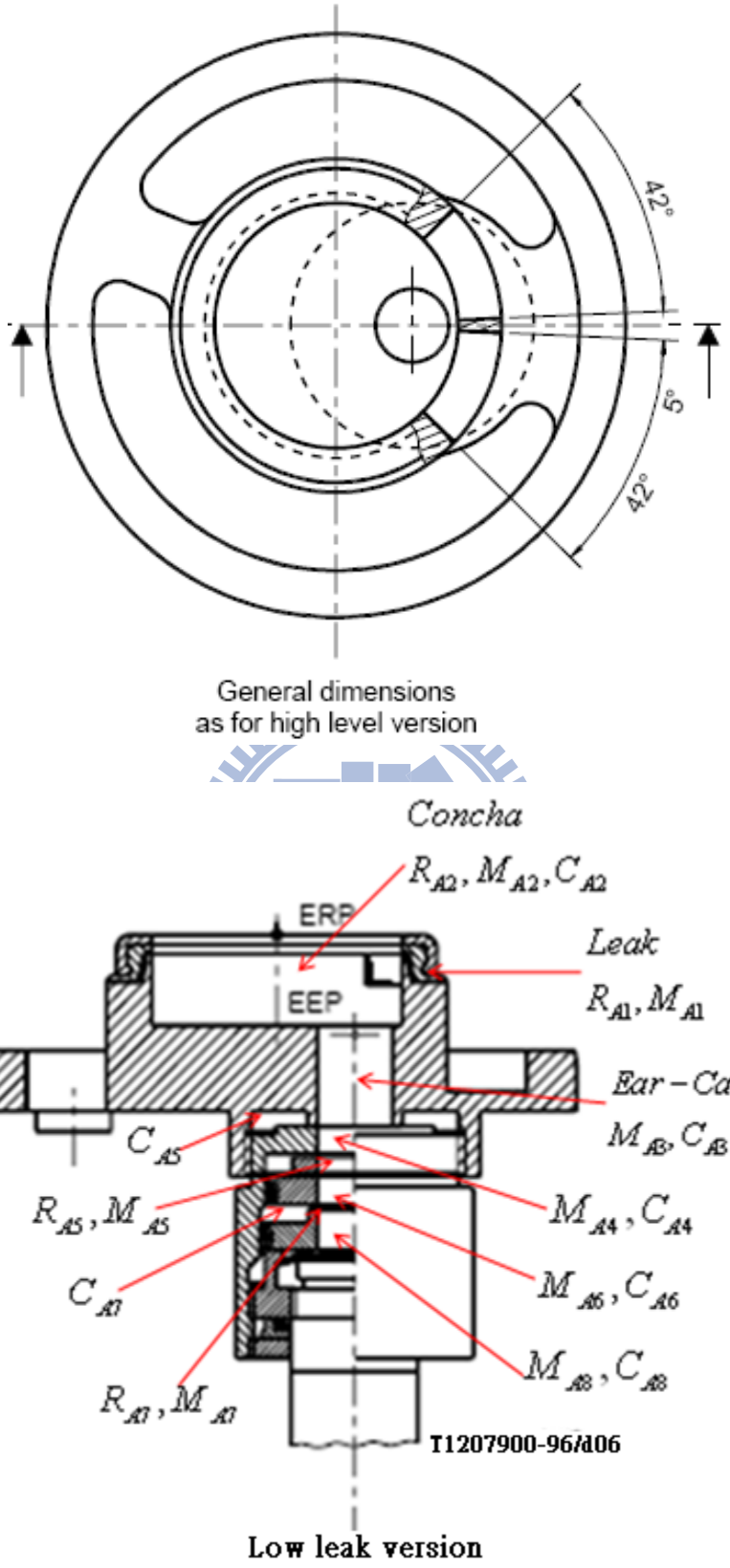

Figure13 The type 3.3 ear simulator. The experiment arrangement and elemental description of type 3.3 ear simulator

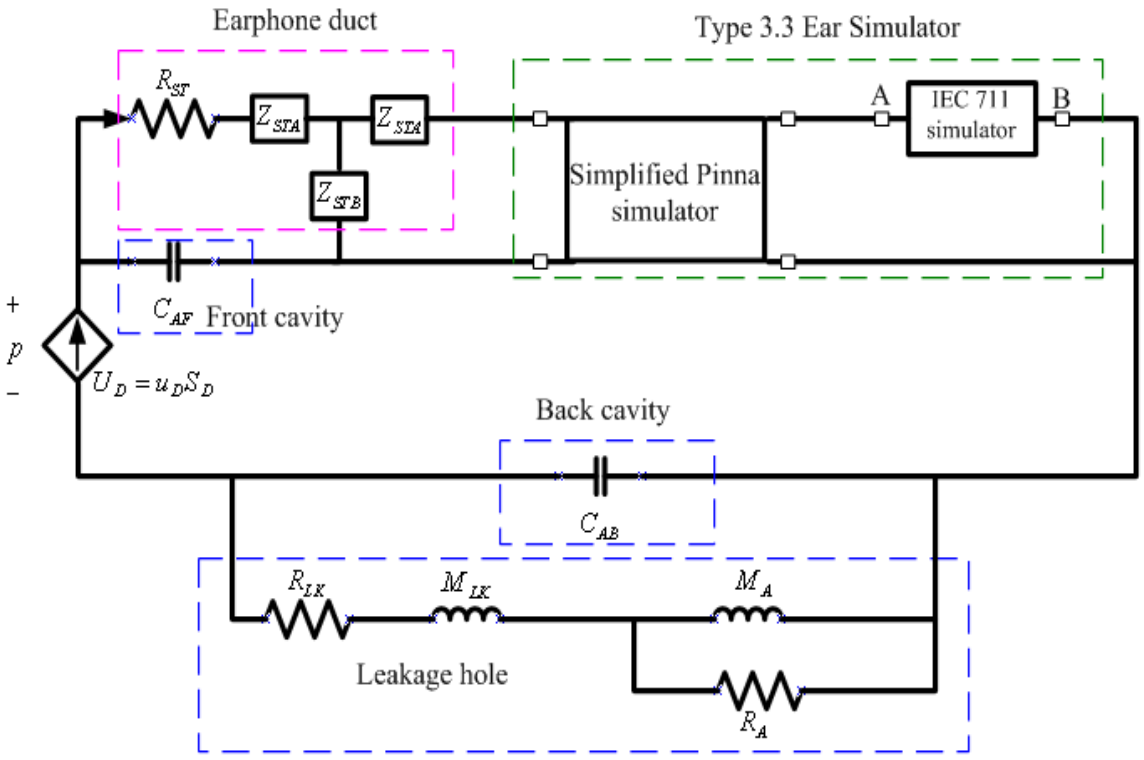

Figure14 The analogous circuit of the acoustical system.

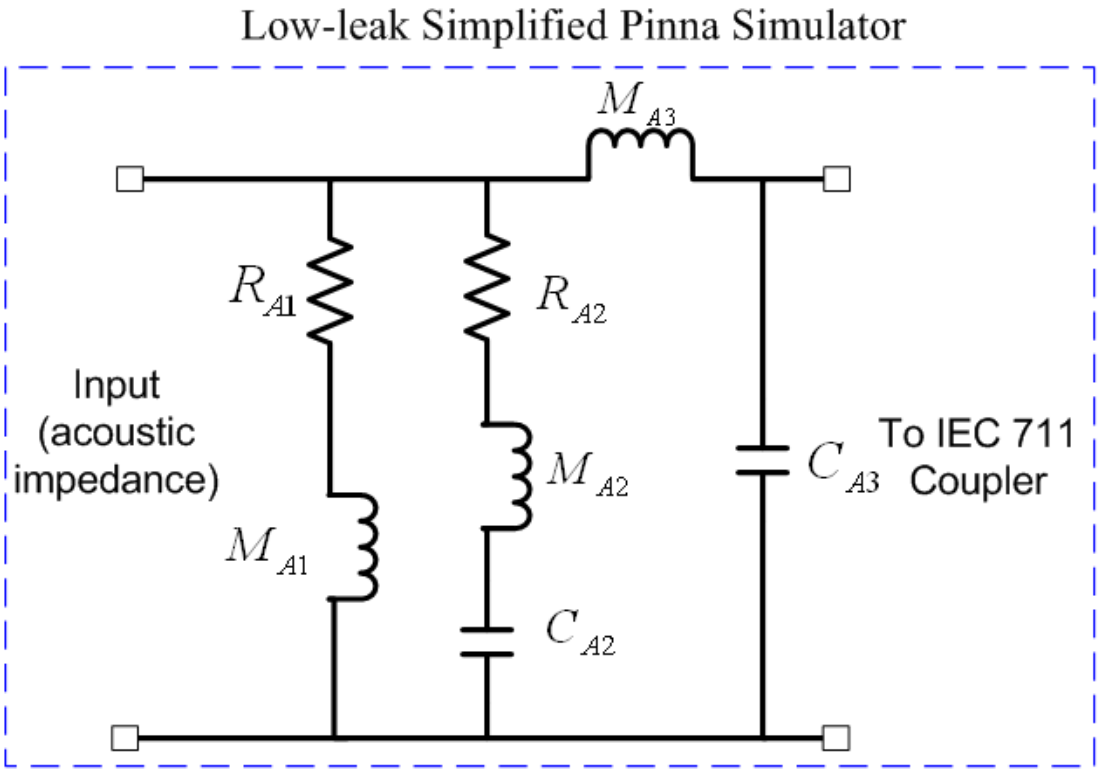

Figure 15 The analogous circuit of the low-leak simplified pinna simulator.

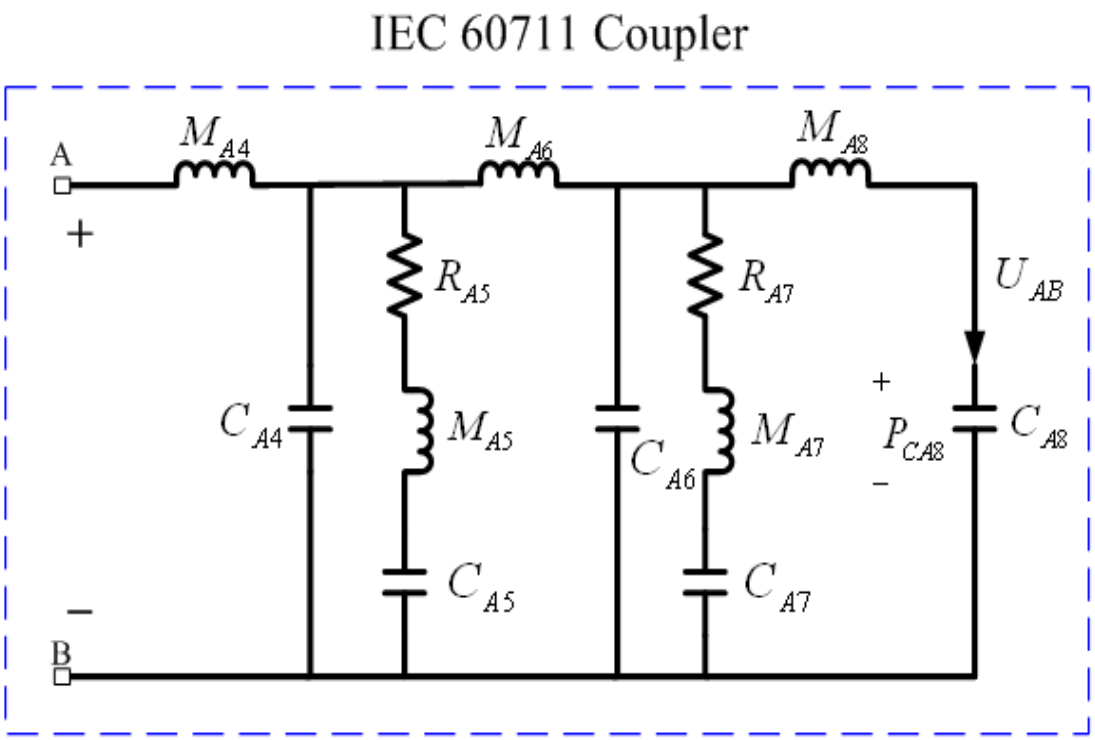

Figure 16 The analogous circuit of the IEC 711 coupler.

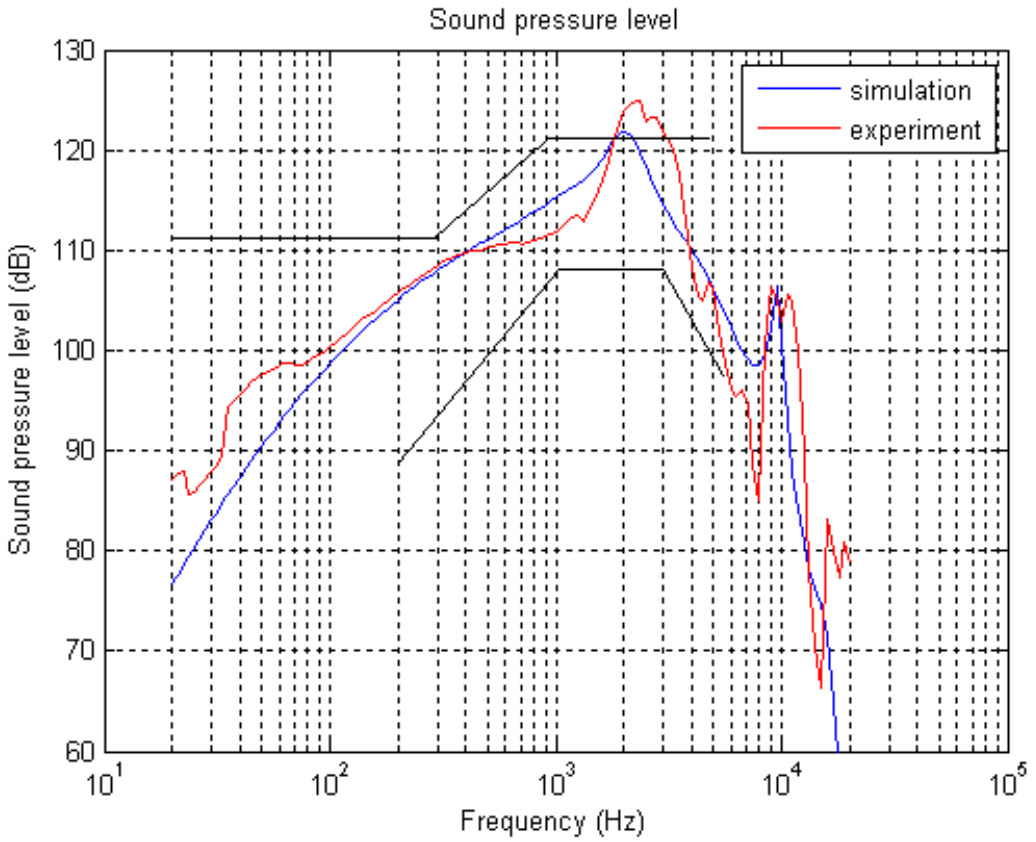

Figure17 The measured and simulated SPL responses for the original non-optimal design. The frequency response mask is shown in the figure.

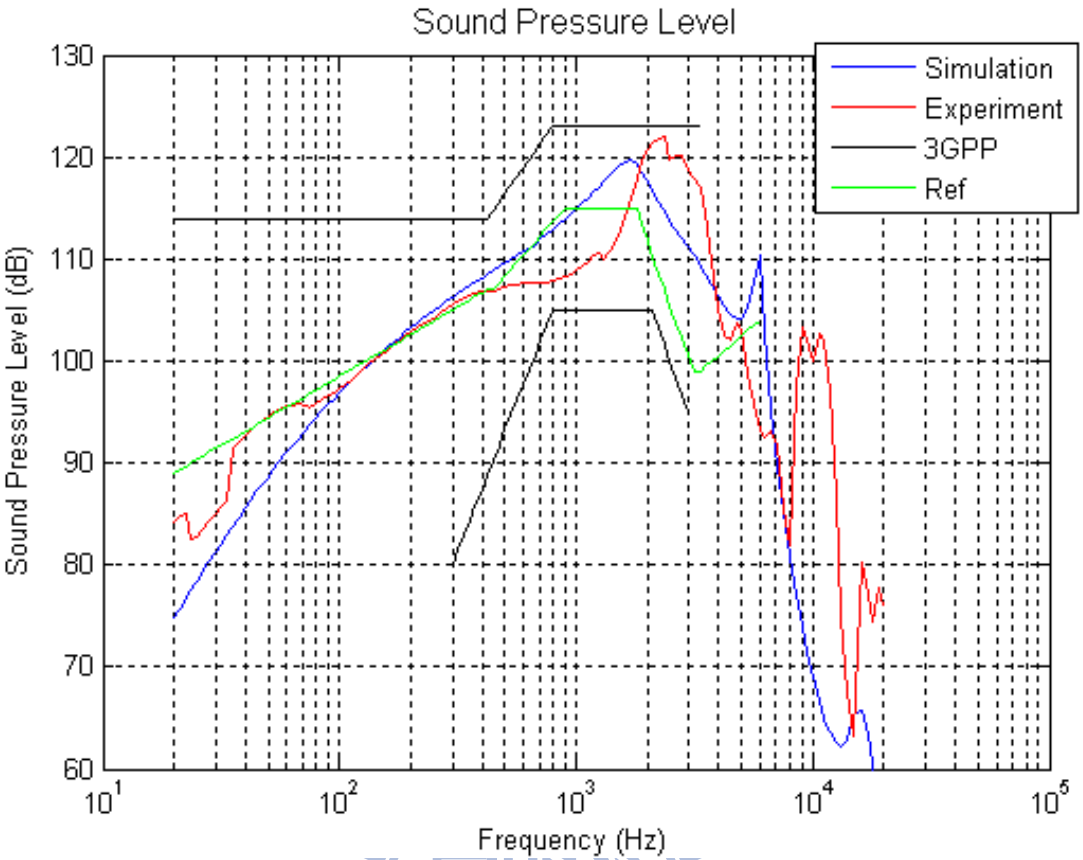

Figure 18 The measured and simulated SPL responses for the original non-optimal design. The frequency response mask and a central reference curve are also shown in the figure.

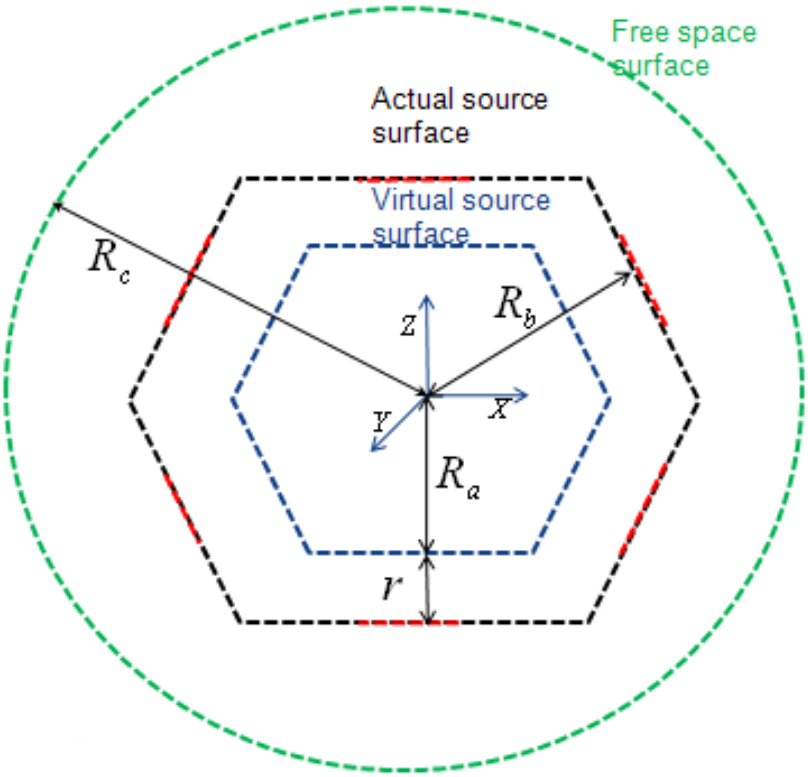

Figure 19 The perspective drawing of dodecahedral source

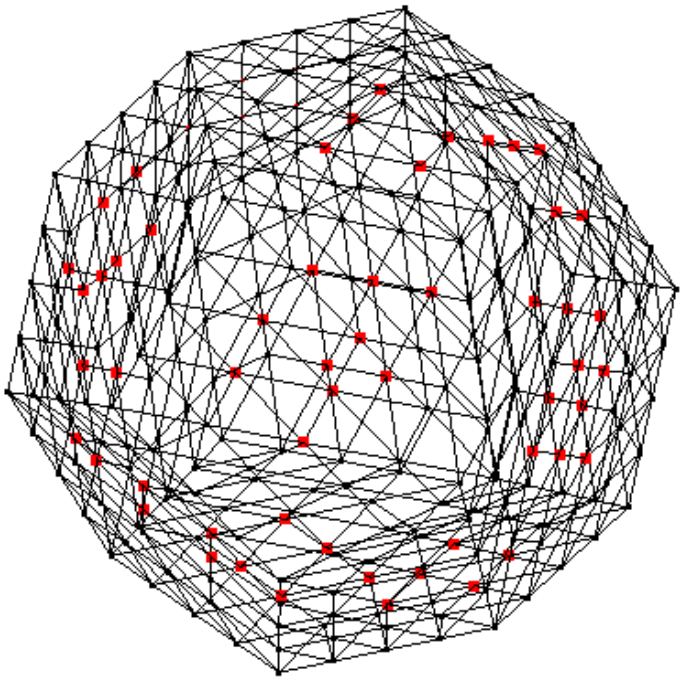

Figure 20 The discrete points on actual source surface.

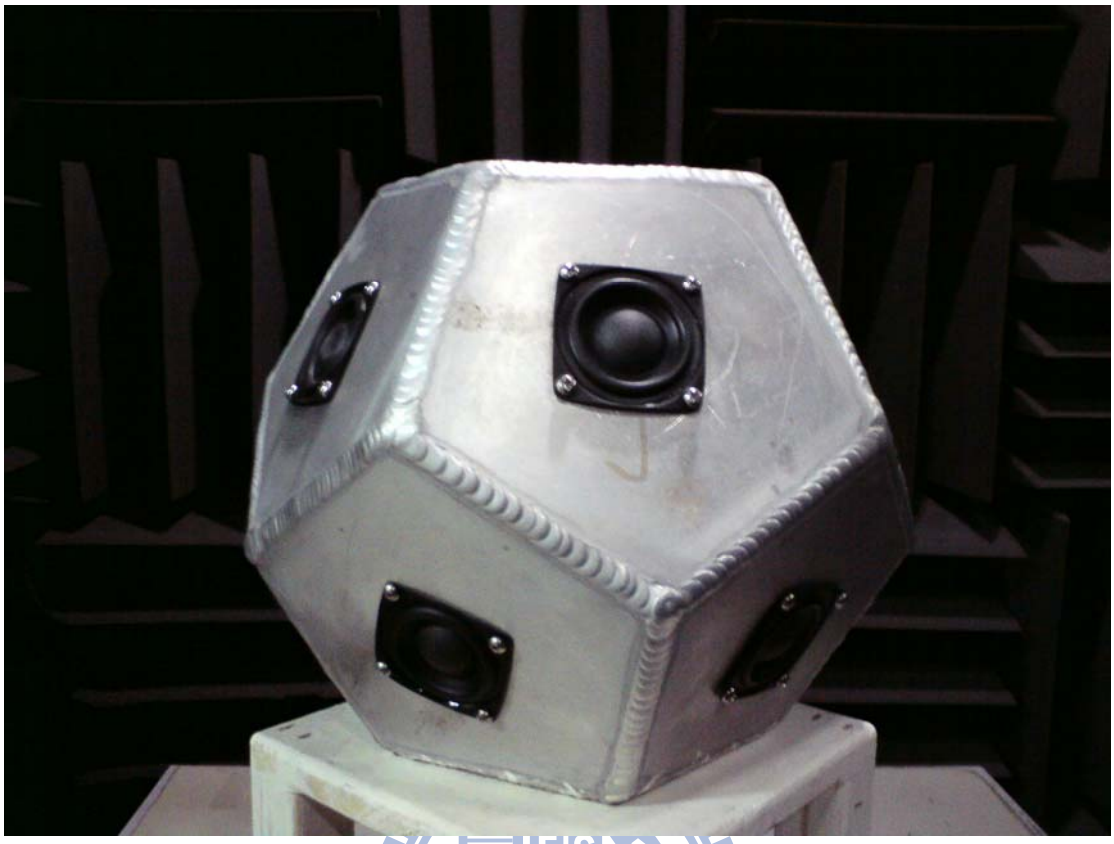

Figure 21 The finished work of dodecahedral speaker.

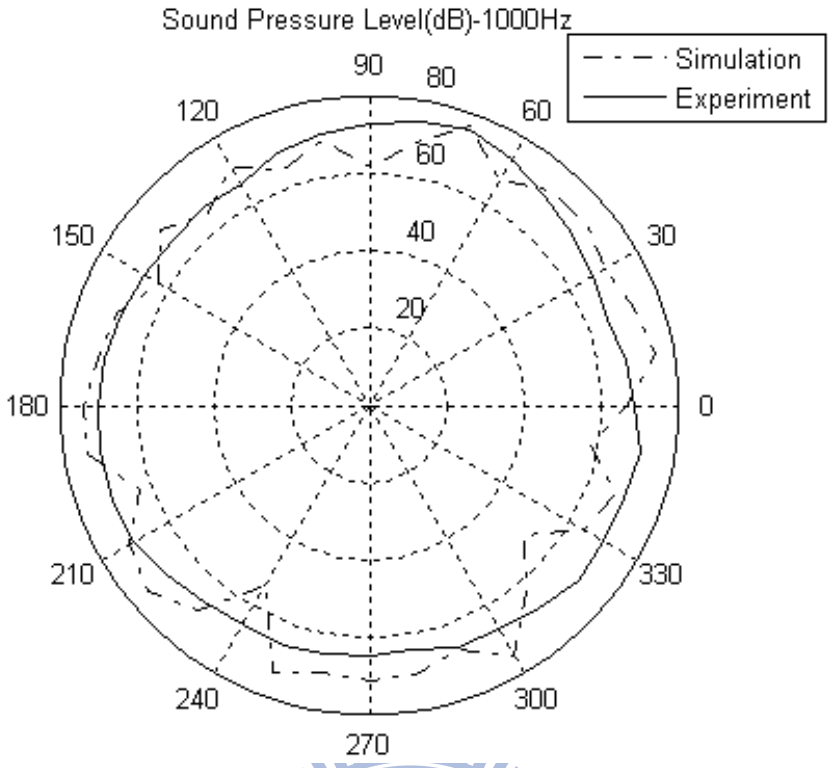

Figure 22 The sound pressure response of simulation and experiment on 1 kHz.

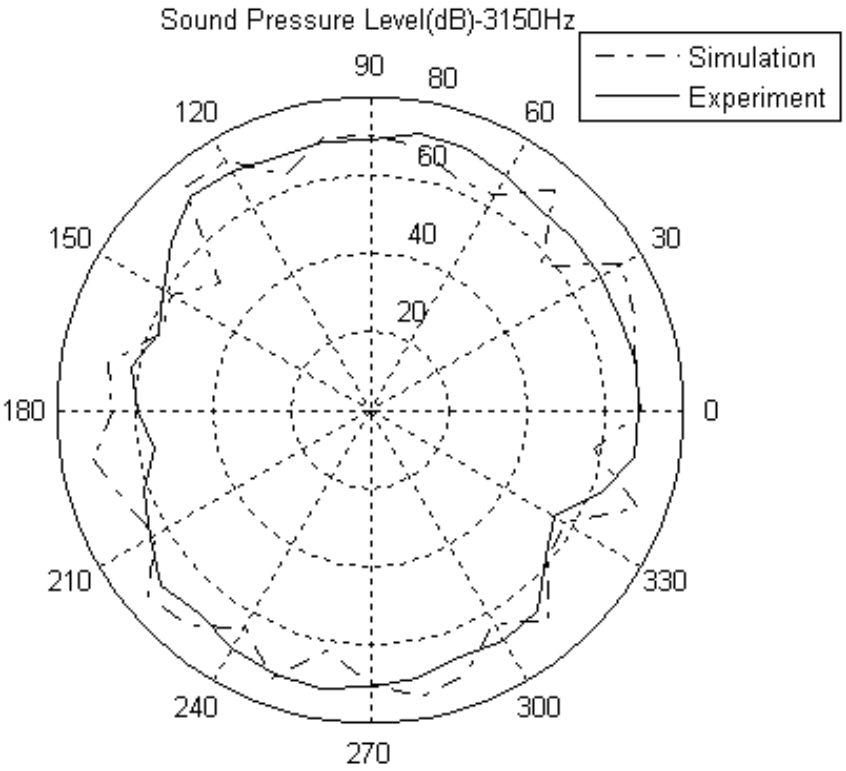

Figure 23 The sound pressure response of simulation and experiment on 3.15 kHz.

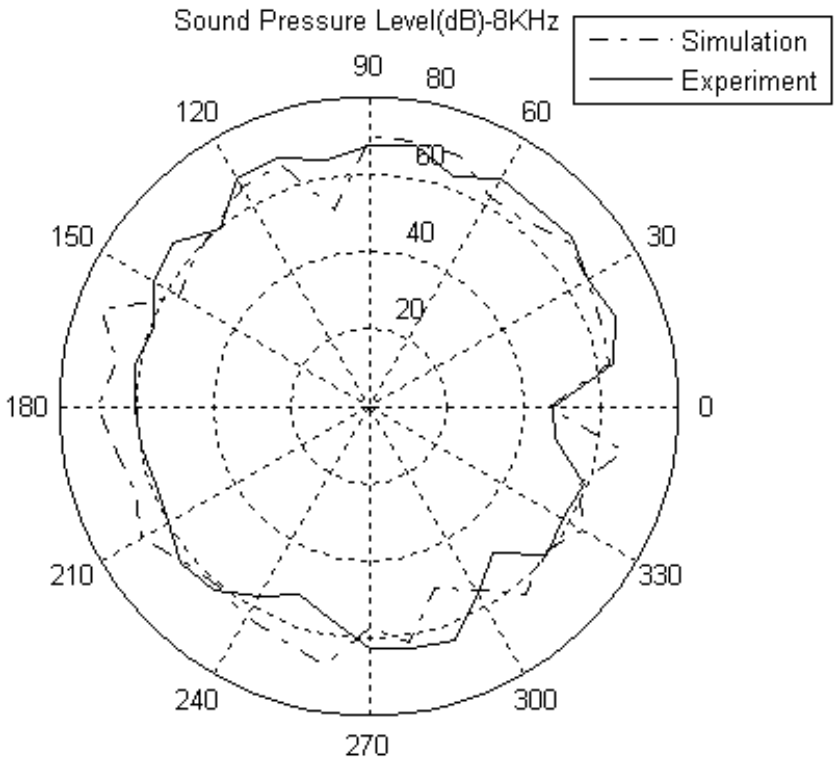

Figure 24 The sound pressure response of simulation and experiment on 8 kHz.

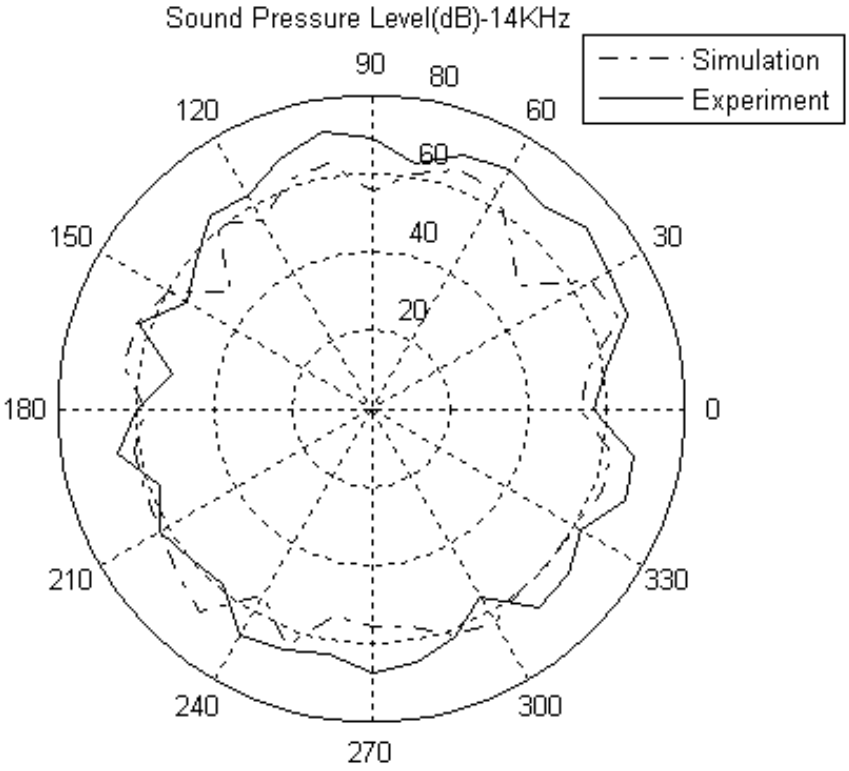

Figure 25 The sound pressure response of simulation and experiment on 14 kHz.

(a)

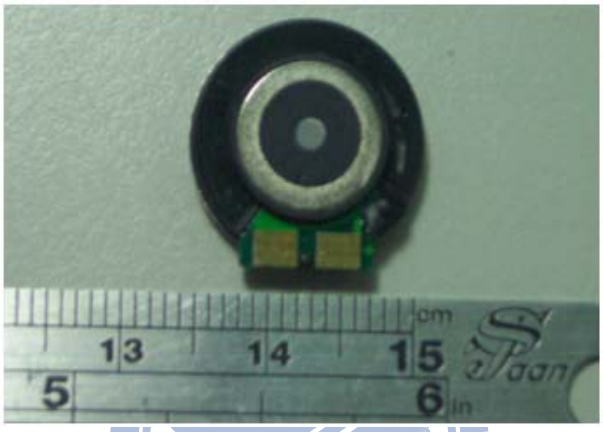

(b)

Figure 26. Photos of a mobile phone microspeaker. (a) Front view (b) Rear view

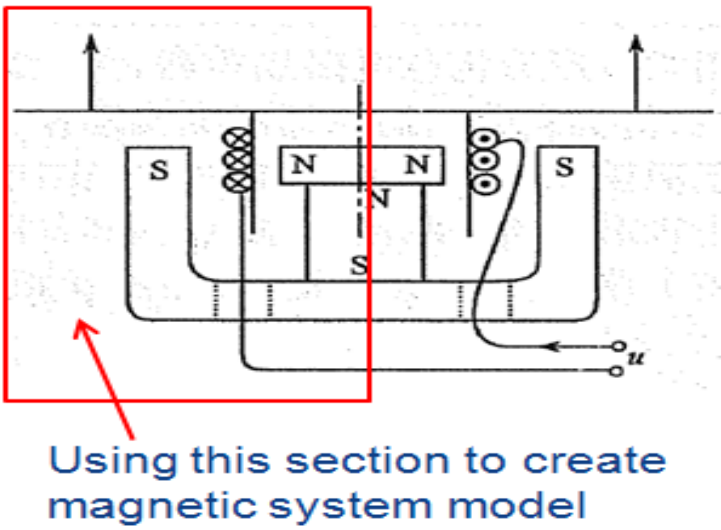

(a)

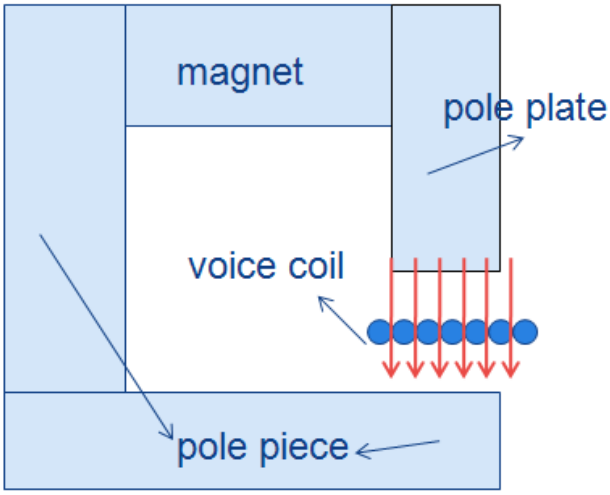

(b)

Figure 27. (a) The cross-section of the voice-coil.
(b) The magnetic system model by using FEA.

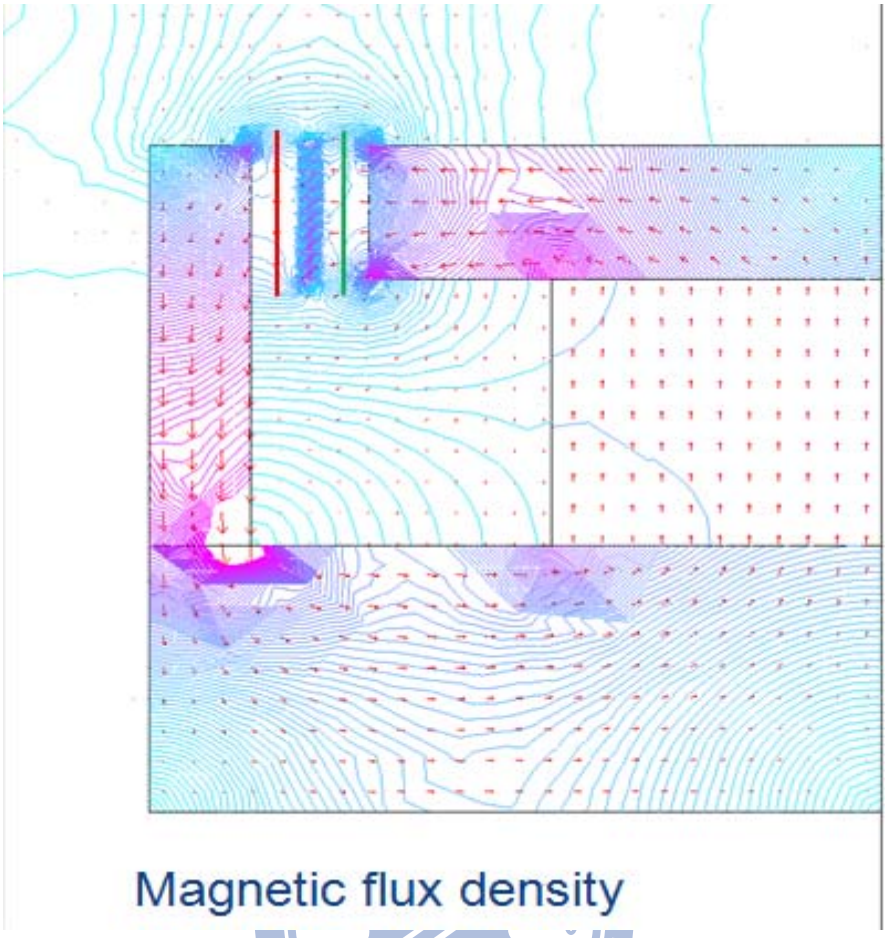

Figure 28 The magnetic flux density of FEA model

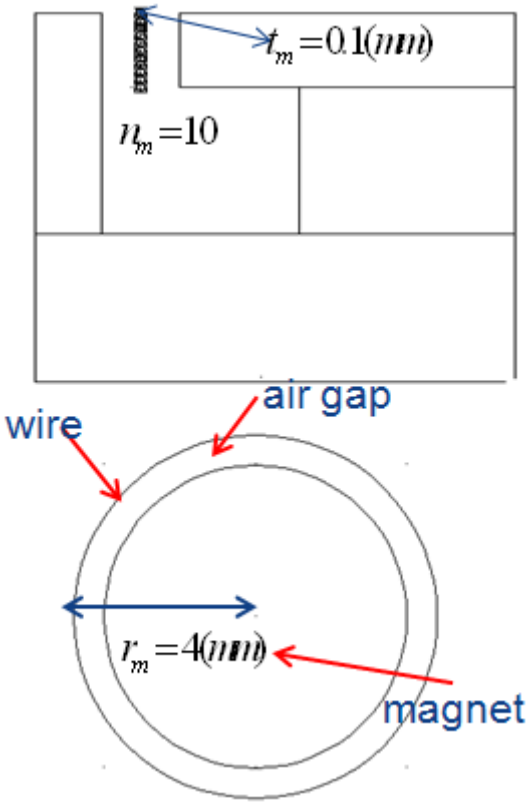

Figure 29 The structure of wire in magnetic system

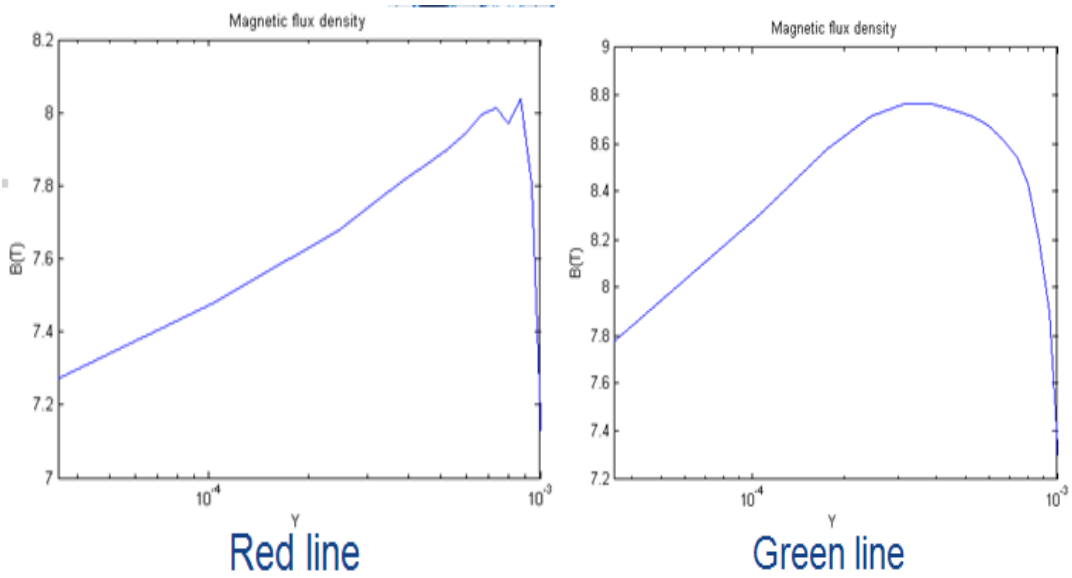

Figure 30 The magnetic flux density on red and green line

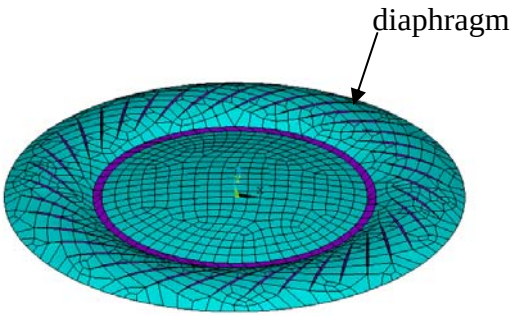

(a)

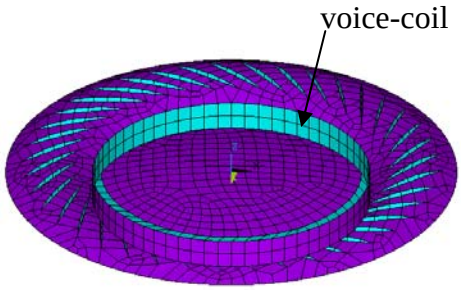

(b)

Figure 31 The finite element model and mesh including diaphragm and voice-coil

(a) top view (b) bottom view

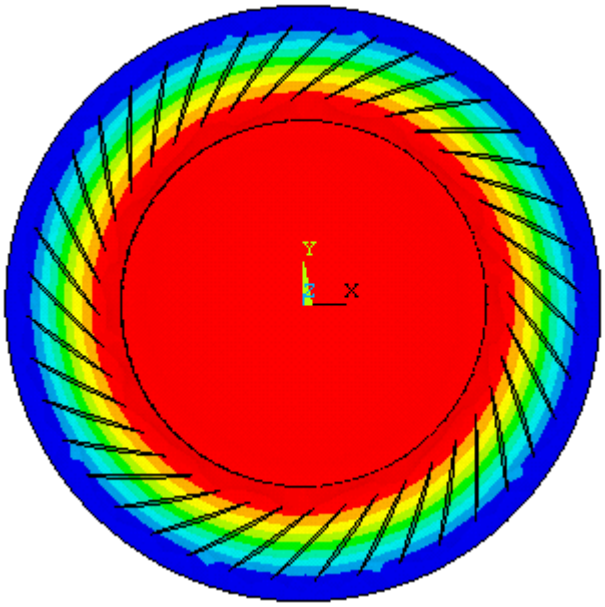

(a)

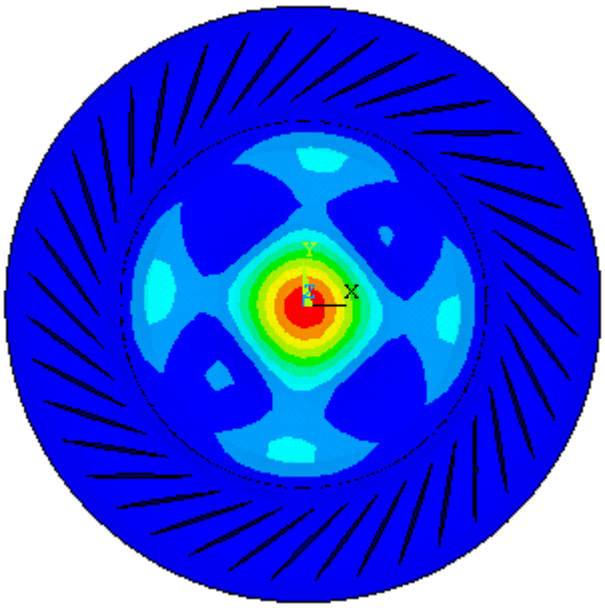

(b)

Figure 32. The results of the modal analysis with mode shape (a) the first piston mode (b) the second piston mode

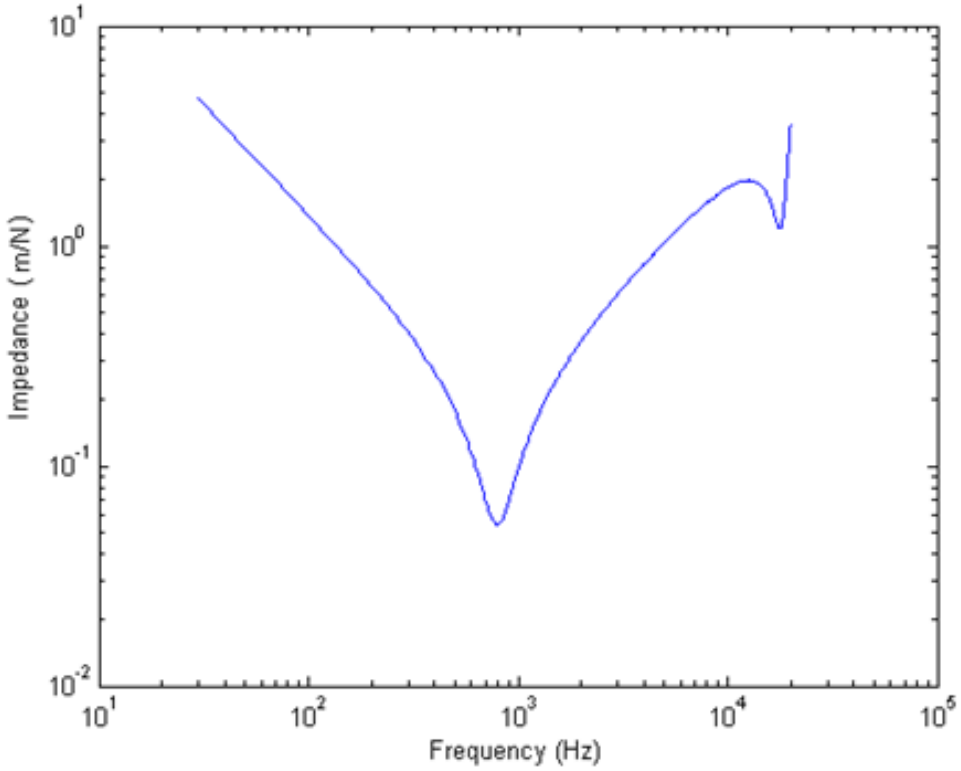

Figure 33 Mechanical impedance of the diaphragm-voice coil assembly Z_{ms}